AMERICAN SOCIETY FOR MICROBIOLOGY | mSystems

Check for updates

| Ecology | Research Article

Metabolomic profiles of stony coral species from the Dry Tortugas National Park display inter- and intraspecies variation

Jessica M. Deutsch,[1] Alyssa M. Demko,[2] Olakunle A. Jaiyesimi,[1] Gabriel Foster,[1] Adelaide Kindler,[1] Kelly A. Pitts,[2] Tessa Vekich,[2] Gareth J. Williams,[3] Brian K. Walker,[4] Valerie J. Paul,[2] Neha Garg[1]

AUTHOR AFFILIATIONS See affiliation list on p. 20.

ABSTRACT Coral reefs are experiencing unprecedented loss in coral cover due to increased incidence of disease and bleaching events. Thus, understanding mechanisms of disease susceptibility and resilience, which vary by species, is important. In this regard, untargeted metabolomics serves as an important hypothesis-building tool enabling the delineation of molecular factors underlying disease susceptibility or resilience. In this study, we characterize metabolomes of four species of visually healthy stony corals, including *Meandrina meandrites*, *Orbicella faveolata*, *Colpophyllia natans*, and *Montastraea cavernosa*, collected at least a year before stony coral tissue loss disease reached the Dry Tortugas, Florida, and demonstrate that both symbiont and host-derived biochemical pathways vary by species. Metabolomes of *Meandrina meandrites* displayed minimal intraspecies variability and the highest biological activity against coral pathogens when compared to other species in this study. The application of advanced metabolite annotation methods enabled the delineation of several pathways underlying interspecies variability. Specifically, endosymbiont-derived vitamin E family compounds, betaine lipids, and host-derived acylcarnitines were among the top predictors of interspecies variability. Since several metabolite features that contributed to inter- and intraspecies variation are synthesized by the endosymbiotic Symbiodiniaceae, which could be a major source of these compounds in corals, our data will guide further investigations into these Symbiodiniaceae-derived pathways.

IMPORTANCE Previous research profiling gene expression, proteins, and metabolites produced during thermal stress have reported the importance of endosymbiont-derived pathways in coral bleaching resistance. However, our understanding of interspecies variation in these pathways among healthy corals and their role in diseases is limited. We surveyed the metabolomes of four species of healthy corals with differing susceptibilities to the devastating stony coral tissue loss disease and applied advanced annotation approaches in untargeted metabolomics to determine the interspecies variation in host and endosymbiont-derived pathways. Using this approach, we propose the survey of immune markers such as vitamin E family compounds, acylcarnitines, and other metabolites to infer their role in resilience to coral diseases. As time-resolved multi-omics datasets are generated for disease-impacted corals, our approach and findings will be valuable in providing insight into the mechanisms of disease resistance.

KEYWORDS comparative metabolomics, Scleractinia, stony coral tissue loss disease, Symbiodiniaceae, tocopherol quinones, acylcarnitines

Coral reefs are an essential component of marine ecosystems, providing habitats for nearly a quarter of ocean life (1, 2), prevent shoreline erosion, and contribute to local economies (3, 4) and cultural practices (5). Climate change and increases of anthropogenic stressors have resulted in an unprecedented increase in the incidence

Editor Justin J. J. van der Hooft, Wageningen University, Wageningen, Netherlands

Address correspondence to Neha Garg, neha.garg@chemistry.gatech.edu.

The authors declare no conflict of interest.

See the funding table on p. 21.

Received 3 July 2024
Accepted 16 October 2024
Published 19 November 2024

of coral bleaching and exposure to diseases (6–9). Diseases may result in coral colony mortality and can drive the local extinction of corals (10). One of the biggest threats to Caribbean reefs is the continued spread of stony coral tissue loss disease (SCTLD). This virulent disease spread rapidly across Florida's Coral Reef over the course of several years, affecting ~22 scleractinian coral species since its first observation in 2014 (11), and has since spread throughout the Caribbean (12). Disease susceptibility, resilience, and lethality vary significantly among affected species (11, 13–16), but underlying mechanisms behind resilience remain unknown.

The Scleractinian (stony coral) coral holobiont is diverse, consisting of the coral animal (host), the endosymbiotic dinoflagellate algae, archaea, bacteria, viruses, and fungi (17–20). Many coral species are sessile organisms that rely heavily on symbiosis with photosynthetic microalgae (Symbiodiniaceae) for their daily energy requirement and through associations with microbial communities for nutrition and defense (17, 21–25). Within the holobiont, multiple interactions occur among all members. The coral animal provides a physical habitat for the endosymbiont and a diversity of microorganisms within the holobiont. Nutrient exchange between the coral host and Symbiodiniaceae includes the exchange of phosphorus and nitrogen (from the coral animal), oxygen, and carbon (from the Symbiodiniaceae, generated through photosynthesis). Studies have shown that Symbiodiniaceae can modulate intra- and interspecies susceptibility to bleaching (26, 27) and disease (28). Metabolite exchange between endosymbiotic zooxanthellae and bacteria influences the fitness of the endosymbiont (29). Bacteria selected by the coral holobiont fulfill several key roles in holobiont metabolite cycling and pathogen defense (30). *Endozoicomonas*, for example, are proposed to provide vitamins to both endosymbiotic dinoflagellates and the coral host (24). The bacterial communities are uniquely structured between the coral skeleton, tissue, and mucus (25). While the microbial community composition within the skeleton and tissue is associated with the coral host species, environmental factors may have a greater impact on the community structure within coral mucus (25). Beneficial bacteria (symbionts) also produce natural products that can provide competitive advantages to the coral holobiont and aid in responding to pathogens (31). Studies that profiled heat-sensitive and heat-tolerant corals have established that symbiosis as well as heterotrophy play a key role in determining which species thrive in the face of increasing ocean temperatures and that endosymbiont identity is an important factor in survival (32–37). Although the cause of SCTLD remains unknown, dysbiosis in the coral holobiont occurs with breakdown in the host-endosymbiont relationship in the gastrodermis resulting in necrosis and opportunistic infections by bacterial pathogens (38). There is also evidence of *in situ* symbiophagy (symbiont degradation) by the coral host in SCTLD-exposed corals (39, 40).

'Omics techniques such as transcriptomics, proteomics, and metabolomics hold promise for delivering insights into biochemical pathways that may drive differences in disease response (41). Pairing multiple 'omics techniques enabled key insights into how *Endozoicomonas* can provide key immune response-related metabolites (such as vitamins) to the coral host and symbiotic zooxanthellae within the coral holobiont (24). Additionally, by comparing transcriptomes of stony corals of species *Acropora hyacinthus* either resilient or sensitive to bleaching stress, the expression of genes important for survival even under non-stress conditions in a phenomenon termed frontloading was observed (42). The differential expression of orthologs related to vesicular trafficking and signal transduction was positively correlated to species-specific susceptibility to SCTLD (39). With advancements in data annotation strategies, untargeted metabolomics is also being increasingly employed to generate, refine, and validate hypotheses to untangle interactions between different members of the holobiont (43, 44). Metabolomics has been largely applied to profile different genotypes of corals (45), locations (46, 47), delineate biochemical pathways important in heat tolerance (48–50), and the effect of environmental factors such as use of sunscreen (51). We compare the findings of these studies to the observations in this work throughout our paper.

We hypothesized that metabolomes of coral species with different reported SCTLD susceptibility would vary in their metabolomes, and such variations could guide future work aimed at understanding of the pathways implicated in disease resilience. The sampling site in this study, Dry Tortugas, Florida, was being monitored regularly in anticipation of SCTLD beginning in September 2020, and the disease was first observed on 29 May 2021. Thus, the species in this study were not affected by SCTLD at the time of sampling (January 2020) but are representative of Florida species that are known to be susceptible to SCTLD. There are only a few investigations that compare metabolic or lipid profiles of field-collected corals that are SCTLD susceptible (41). With the unabated spread of SCTLD along the Florida reef, opportunities to profile inter and intraspecies variation in metabolomes ahead of disease and post disease were envisioned to generate testable hypotheses to delineate biochemical pathways underlying disease susceptibility. To test our hypothesis and compare metabolomes of coral species with different SCTLD susceptibilities, we collected healthy coral fragments of four coral species, *Orbicella faveolata*, *Montastraea cavernosa*, *Meandrina meandrites*, and *Colpophyllia natans*, ahead of the SCTLD front in the Dry Tortugas. *M. meandrites* and *C. natans* are highly susceptible to SCTLD, while *O. faveolata* and *M. cavernosa* are defined as moderately susceptible (13, 15, 16). SCTLD susceptibility is defined by the length of time between the disease's arrival to a reef and observation of lesions on a particular species, rates of lesion progression, and prevalence among species (15, 16). *M. meandrites* was one of the first reported species affected in the Dry Tortugas (52), while *C. natans* recruits spawned from parents in the Dry Tortugas showed *ex situ* lesion progression rates of 24.9-31.1%/day, which is in range for highly SCTLD susceptible corals (53). The Dry Tortugas is a unique habitat for corals along the Florida coral reef system where species such as *Acropora palmata*, *Siderastrea siderea,* and *Porites astreoides* have exhibited faster growth rates and enhanced reproduction relative to conspecifics in the Florida Keys (54). This may be attributed to oceanographic conditions that drive periodic upwelling, which is favorable for heterotrophy, and cooler temperatures and greater distance from urbanization and sources of pollution (54). Exogenous untargeted metabolome profiles of Dry Tortugas' seawater samples were previously reported to be distinct from the profiles of seven other zones within Florida's Coral Reef prior to SCTLD arriving at the Dry Tortugas (46). Thus, the visually healthy corals in this study from the Dry Tortugas provided the unique opportunity to examine and compare the metabolomes of several coral species growing under optimal growth conditions in Florida (54–56) before this region was affected by SCTLD.

In this work, we apply an untargeted high-performance liquid chromatography-mass spectrometry (LC-MS)-based approach to profile the metabolomes of a small sample set of four coral species (*M. meandrites*, *C. natans*, *O. faveolata*, *M. cavernosa*) utilizing recently developed advanced compound annotation methods to identify metabolites underlying the interspecies differences observed. While metabolomics analysis has been performed on Caribbean Scleractinian corals (43, 45, 46, 57–61), our understanding of differences between the metabolomes of visually healthy Caribbean stony coral species is limited. Thus, we seek to address this gap in knowledge by describing chemical classes that are variably detected between four visually healthy coral species from the Dry Tortugas National Park sampled in January 2020 (52). In this study, we identify an endosymbiont-derived vitamin E pathway and a host-derived acylcarnitine pathway that were significantly variable among species. We describe additional chemical diversity by partitioning the crude extract of whole coral. Lastly, we report differences in the bioactivity of partitioned extracts of whole corals against bacterial pathogens.

RESULTS AND DISCUSSION

Inter- and intraspecies variation in metabolome profiles

Metabolome extracts from four stony coral species (*Orbicella faveolata*, *Monstastraea cavernosa*, *Meandrina meandrites*, and *Colpophyllia natans*) were subjected to LC-MS analysis (Fig. 1; Table S1). The resulting data were analyzed using a variety of data

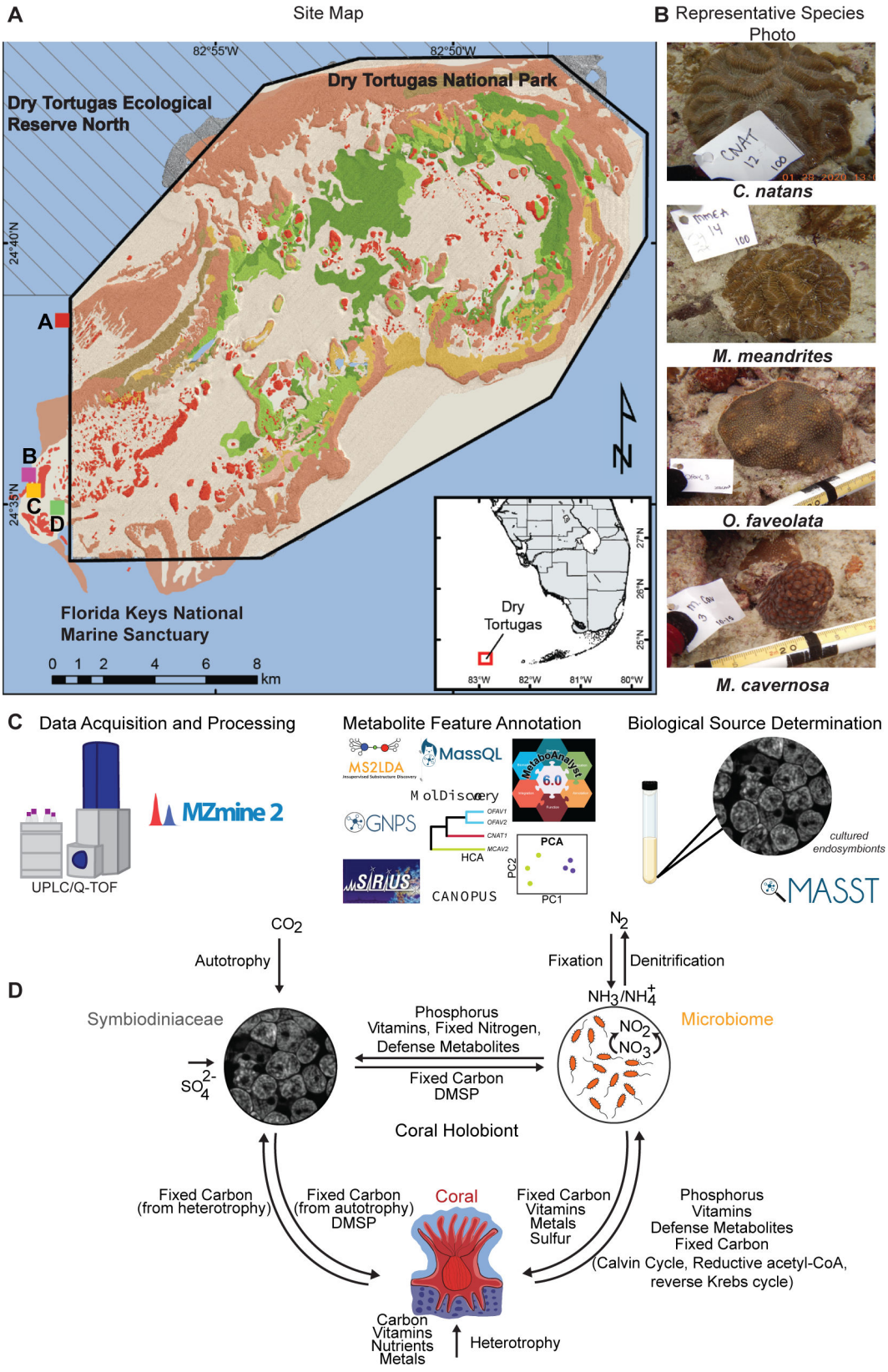

FIG 1 Sample collection, data acquisition, and analyses. (A) Benthic map of the sample sites in relation to Dry Tortugas National Park. Colors denote the benthic habitats (partially transparent) overlaid on high-resolution bathymetry. Red and brown illustrate coral reef habitat (Florida unified reef map, Florida Fish and Wildlife Conservation Commission, 2016). A, B, C, D refer to the sites at which coral colonies were sampled. Coordinates for these sites are in

(Continued on next page)

Fig 1 (Continued)

Table S1. (B) Representative photographs of each coral species in this study (CNAT = *C. natans*, MMEA = *M. meandrites*, OFAV = *O. faveolata*, MCAV = *M. cavernosa*). (C) Untargeted metabolomics data were acquired, processed, and analyzed with a variety of methods. Metabolomics data available through public data sets (mined using MASST) and acquired on cultured algae was used to assign the biosynthetic source of annotated metabolite features. (D) Schematics of representative interactions between the coral holobiont members are shown. The host genotype, the microbiome composition, and the endosymbiont Symbiodiniaceae species as well as the complex interplay of interactions between them can confer resilience to the increased frequency and impact of coral diseases.

visualization and metabolite annotation tools (Fig. 1C). Unsupervised principal component analysis (PCA) revealed that metabolome profiles of *M. meandrites* had the lowest intraspecies variation compared to the other coral species (Fig. 2A). The largest interspecific separation captured on the first principal component (PC) was observed between *M. meandrites* and *M. cavernosa*. Four PCs captured interspecies variation between *M. meandrites* and the other species, and intraspecies variation for *M. cavernosa* (Fig. S1A through E). The largest intraspecies distribution on PC1 was observed for *C. natans*, followed by *O. faveolata* and *M. cavernosa*. While the metabolomes of *M. cavernosa* fragments were spread across PC2, tighter clustering was observed for the other species along this component. PCs 3 and 4 captured metabolome variation between individual extracts, revealing that additional factors beyond species are captured within the metadata analysis (discussed further below) (Fig. S1A through E). We calculated alpha and beta diversity for each coral (using Shannon entropy and Brays-Curtis similarity metrics, respectively, Fig. S2) to quantify metabolome similarity. A principal coordinates analysis on the Bray-Cutis similarity matrix constructed on the metabolome data revealed tighter clustering for *M. meandrites,* while the other species were spread along the first principal coordinate (Fig. S2A). The within species beta diversity was significantly larger than beta diversity between species (Fig. S2B, Mann Whitney *U* Test, $P = 0.00082$), further supporting that the metabolome analysis captures variation driven by factors beyond coral species. There was no significant difference between the alpha diversity for each species found using a Kruskal Wallis Test (Fig. S2C, $P= 0.119$).

Using permutational multivariate analysis of variance (PERMANOVA) (62), we found metabolome variation differed significantly across coral species (*Pseudo-*$F_{3,13} = 2.192$, $P = 0.007$), with no significant effect of site (as a random effect, $P = 0.670$). We queried whether SCTLD susceptibility categorization (OFAV, MCAV = moderate; CNAT, MMEA = high) affected metabolome variation. We could not examine interactive effects due to a lack of Susceptibility × Species replication. We performed PERMANOVA with susceptibility as a single fixed factor and found that metabolome variation was significantly different between the two groups (*Pseudo-F* = 3.191, $P = 0.001$). Additionally, a model with susceptibility as a fixed factor and species as a random effect found that Species(Susceptibility) was slightly significantly different (*Pseudo-*$F_{1, 2} = 1.715$, $P = 0.021$). Therefore, both coral species and SCTLD susceptibility affect metabolome variation, but it is unclear how the two interact in affecting metabolome differences. We cannot fully disentangle the effects of species and susceptibility with the current sampling regime in this study; therefore, such efforts are an important avenue for future inquiry. Sampling species with moderate resilience (i.e., some individuals are susceptible, others never develop lesions) where both affected and unaffected colonies were sampled would be a potential way to disentangle this effect. A non-metric multi-dimensional scaling (nMDS) plot by species was constructed to visualize metabolome variation using a method appropriate for smaller sample sizes. The nMDS plot divided the samples into four distinct clusters. Consistent with the PCA, all *M. meandrites* samples clustered together in one group, and a larger spread was observed for other species with metabolomes of *M. cavernosa* displaying the largest intraspecies variation (Fig. S3). These observations aligned with previous findings where apparently healthy *M. cavernosa* from a SCTLD endemic site in Broward County showed similar intraspecies variation (43). The proximity between *M. cavernosa* colonies on the reef in this previous study explained the variation

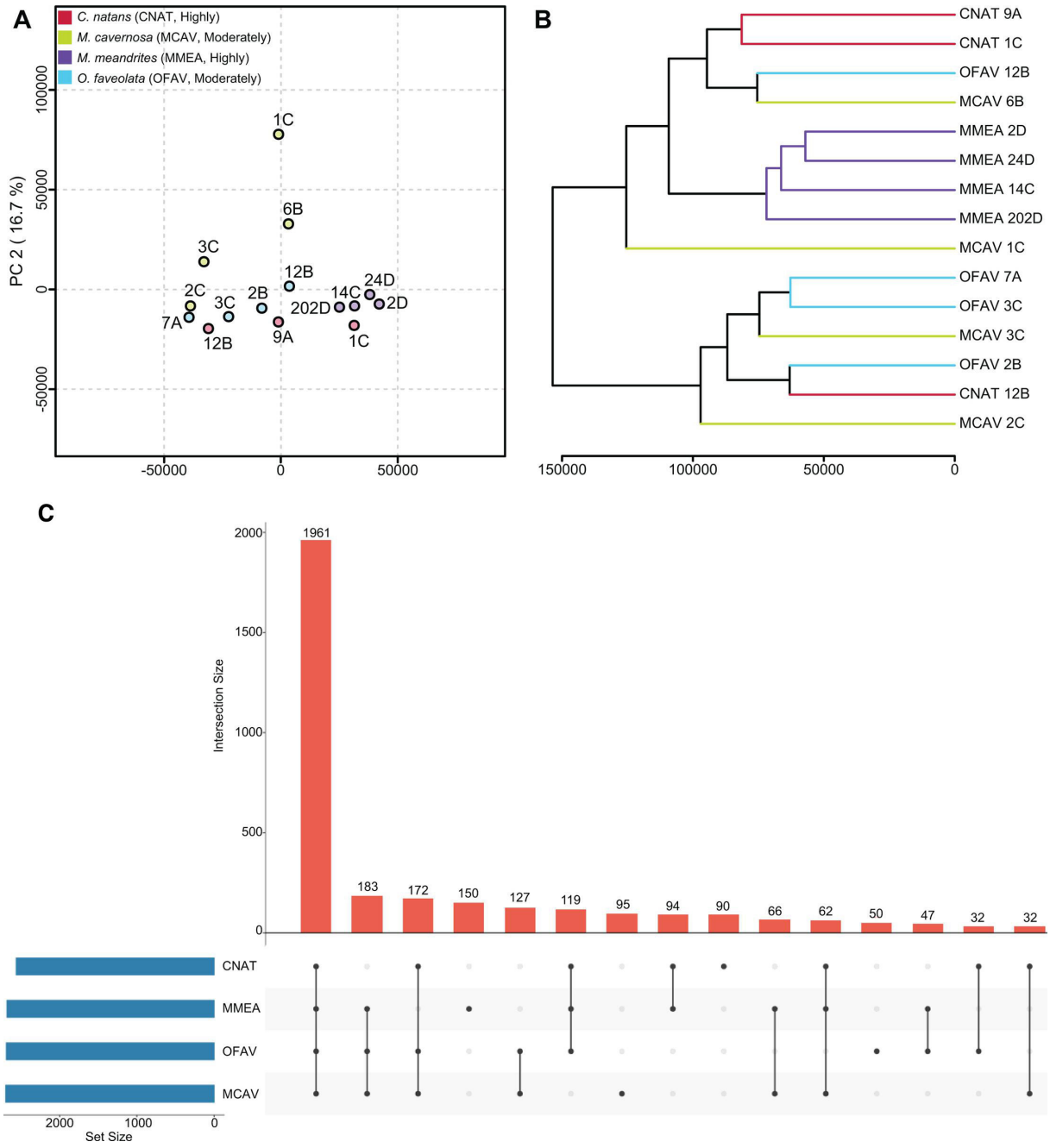

FIG 2 Intra- and interspecies variation of metabolomics data. (A) Principal component analysis of corals: *C. natans* (CNAT, red), *M. cavernosa* (MCAV, green), *M. meandrites* (MMEA, purple), and *O. faveolata* (OFAV, blue). The SCTLD susceptibility categorization is included in the key ("Highly," "Moderately"). Axes are labeled with the corresponding variance explained by each principal component. A, B, C, D refer to the site from which the coral was sampled (Table S1). (B) Hierarchical clustering analysis reveals a separate cluster for all *M. meandrites* samples, while the other species are distributed across clades. Colored branches correspond to species as outlined in (A). The letter at the end of the sample name corresponds to the sampling site. The *x*-axis represents the distance between the samples/clades. (C) UpSet Plot showing the distribution of detected metabolite features. The number above each bar represents the number of features in that intersection. "Set Size" denotes the total number of features detected in each coral species. The inset table includes a number of features detected within each species, as well as the number of annotated features reported in this paper.

in some instances but did not completely explain the metabolome variation observed for *M. cavernosa* in Broward County (43). The beta diversity analysis conducted in this study revealed three pairs of corals from the site B or D as having the greatest Bray-Curtis similarity score to each other. These include OFAV2B/CNAT12B, MCAV6B/OFAV12B, and

MMEA2D/MMEA24D. Thus, we see further evidence of reef site driving metabolome similarity in some instances although for the MMEA pair we cannot disentangle the effect of site and species on the metabolome similarity.

An unsupervised hierarchical clustering analysis (HCA) revealed *M. meandrites* was the only species that clustered within a single clade (Fig. 2B, purple branches), further indicating the relatively low intraspecies variation. The HCA also reveals that the corals within the aforementioned pairs identified through the Bray-Curtis similarity analysis have the greatest metabolome similarity to each other (Fig. 2B). There was significant variation in metabolomic variation (multivariate dispersion) among the coral species ($F_{1,3}$ = 7.944, P = 0.045). Overall, MCAV was the most variable (average distance to group centroid = 33.3) with the variation being significantly higher than the variation observed for MMEA (average distance = 19.2, P = 0.036). OFAV was the second most variable (average distance = 29.3) and the variation was significantly higher than the variation of MMEA (P = 0.030). The relative metabolomic variation did not differ between pairwise comparisons performed for other coral species. This phenomenon has been observed in deep sea corals where interspecies differences rather than site-dictated clustering of metabolite profiles (63). However, intraspecies differences may be attributable partially to site, as Haydon and colleagues found metabolite differences in *Pocillopora acuta* based on reef site, even after acclimation of the corals in aquaria as is the case in this study (48). Thus, when comparing multiple species of corals from different reef sites, replication of species collected from each site should be conducted where possible. The intraspecies metabolomic variation observed in this study may further be partially explained by different genotypes (45), and both intra- and interspecies variation may be influenced by the endosymbiotic profile, microbial community, bleaching history, and stimuli/stressors unique to the sampling site (21, 22, 64, 65). Acquiring data on seawater (exometabolomics), cataloging abiotic factors at reef sites, and profiling the endosymbiont and microbial community will aid in disentangling what additional factors drive metabolome variation. In a metabolomics study of cultured *Symbiodinium* species, Klueter et al. noted that metabolite profiles varied by species and the degree of metabolome variation was not ubiquitous across species given the different classification error rates of each symbiont species (66). The distinct metabolome profiles of *M. meandrites* compared to the other corals species in this study could be influenced by the symbiont types of the coral species. The *M. meandrites* sampled for this study may host symbionts with highly similar metabolomes or interaction networks with the associated microbiome, while the other coral species may host symbionts and/or microbiome with more diverse metabolomes. Incorporating microbiome analysis and symbiont typing into metabolome studies would be beneficial toward delineating how the degree of observed metabolome variation may correspond to the symbiont and the microbiome species present. Another factor that may contribute to the intraspecies metabolome variation captured in this study is cryptic lineages observed within the studied species (67). Cryptic coral species lineages may share phenotypic traits but have distinct underlying genomic differences (67). *M. cavernosa* (68, 69) and *O. faveolata* (70, 71) are reported to have cryptic lineages. The genomic differences between the coral hosts imply a strong possibility for metabolite differences (since the metabolome reflects the functional biochemical state of the system, in this case the coral holobiont). Proven association with different symbiont genera [reported for *O. faveolata* (70)] and potential association with different microbial assemblages (yet to be studied for the species in this report) among cryptic lineages could further diverge metabolome profiles, as all the members of the coral holobiont influence and contribute to the metabolome. Such phenomena (67) may well explain the metabolome variation of *M. cavernosa* and *O. faveolata* in this study, and although cryptic lineages have not yet been identified for *Colpophyllia* (67), the observed metabolome variation in *C. natans* may be partially explained by this as well.

The UpSet Plot generated to show the distribution of metabolite features revealed the greatest number of unique features were detected in *M. meandrites* extracts,

followed by *M. cavernosa*, *C. natans*, and *O. faveolata* (Fig. 2C). Since the statistical analyses revealed a distinct metabolome profile for *M. meandrites* and a greater intraspecies metabolite variation captured for the other coral species, unique features present in *M. meandrites* and features that were variably detected among *M. meandrites* and other coral species were prioritized for annotation and are described below.

Metabolite features driving variation

Vitamin E family compounds as potential biomarkers of stressor susceptibility

A metabolite feature *m/z*_RT (*m/z*: mass to charge, RT: retention time in min) 449.398_21.3 min, uniquely detected in *M. meandrites* extracts, was proposed as α-tocopherolhydroquinone by the *in silico* annotation tool MolDiscovery. SIRIUS with CSI:FingerID also proposed the annotation for this feature as α-tocopherolhydroquinone. We searched for α-tocopherolhydroquinone spectra in the literature and used MS^2 spectral matching with a published spectrum (72) of silicated α-tocopherolhydroquinone to further support the annotation (Fig. S4A). This feature clustered in Feature Based Molecular Networking (FBMN) analysis with another feature at 447.383_21.3 min representing one unsaturation from α-tocopherolhydroquinone ($\Delta m/z$ = 2.015). We annotated this feature as α-tocopherolquinone, the oxidation product of α-tocopherolhydroquinone (73, 74) and confirmed this annotation with an analytical standard of α-tocopherolquinone (Fig. S4B and C). To identify additional metabolites, we applied unsupervised substructure discovery using MS2LDA (75) (Fig. 3A; Table S2).

It is interesting to note that α-tocopherolquinone, an oxidation product of α-tocopherol (76, 77), and α-tocopherolhydroquinone were exclusively detected in highly SCTLD susceptible *M. meandrites* and *C. natans* but not in *O. faveolata* and *M. cavernosa* with moderate SCTLD susceptibility (15, 16). These features were also not detected in the

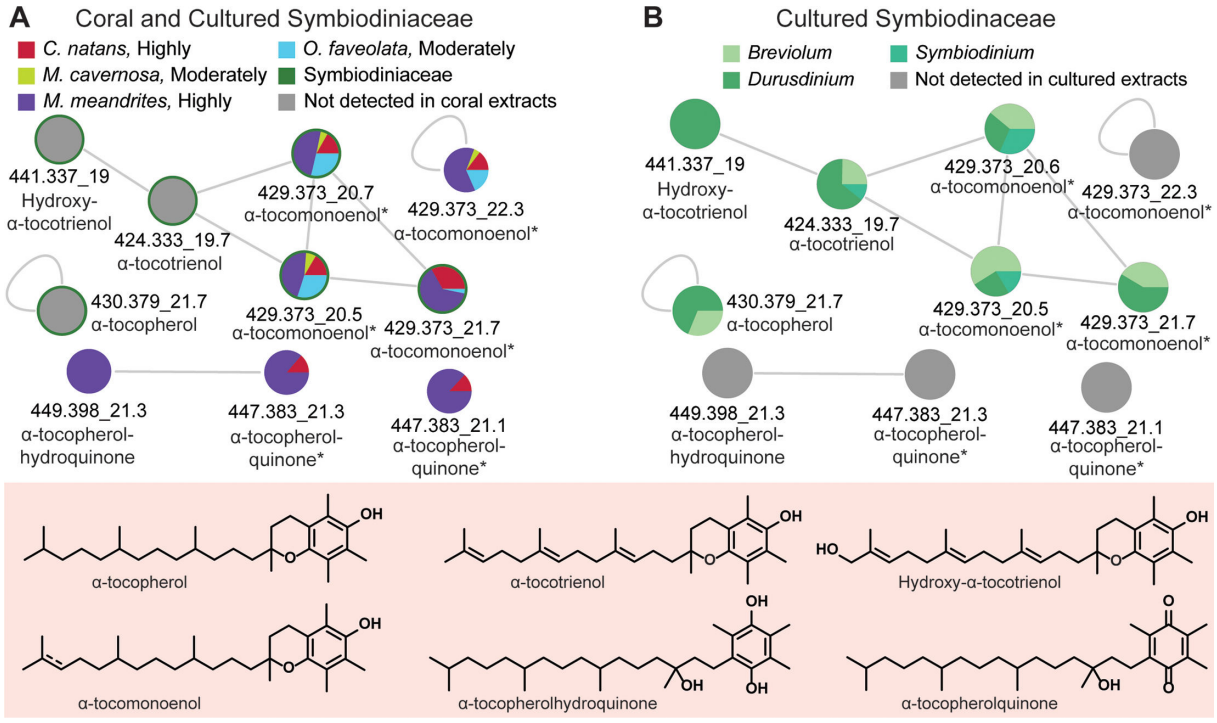

FIG 3 Analyses of vitamin E family compounds. (A) Network of annotated vitamin E family compounds with *m/z*_RT (*m/z*: mass to charge, RT: retention time in min). The * indicates these features have identical MS^2 spectra, but different retention times, representing isomeric species. (B) The detection pattern of annotated vitamin E family compounds in cultured endosymbiont extracts. The comprehensive list for annotated vitamin E family compounds is provided in Table S2, and MS^2 mirror plots supporting annotations of tocopherol(hydro)quinone are provided in Fig. S4. The SCTLD susceptibility categorization is included in the key ("Highly," "Moderately").

extracts of cultured Symbiodiniaceae included in this study (Fig. 3B). The *Durusdinium*-associated mangrove coral *Pocillopora acuta* was previously reported by Haydon and colleagues to accumulate α-tocopherol in summer (48). This observation was suggested as a possible mechanism of "frontloading" associated with the resilience of *Durusdinium*-associated corals (48). Tocopherols are the most prominent antioxidants that counteract lipid peroxidation. Using transcriptomics, the gene for arachidonate 5-lipoxygenase (ALOX5) was found to be significantly differentially expressed with its highest expression in the most susceptible corals, including *C natans* (39). ALOX5 is a key enzyme in mediating lipid peroxidation (78) which can lead to cell death such as apoptosis, ferroptosis, and pyroptosis (78). Thus, we searched the literature to identify studies that might link α-tocopherol(hydro)quinones with lipid peroxidation and cell death. While linking specific metabolites with processes is outside the scope of this study, we can speculate on possible functions of metabolites and determine future avenues of inquiry based on literature precedence. Indeed, a recent report updated the mechanism of action for iron-dependent anti-apoptotic activity (ferroptosis) of α-tocopherol (79). Tocopherol was suggested to be the pro-vitamin E form, while the (hydro)quinone forms produced from the oxidation of α-tocopherol were shown to be the activated forms responsible for the prevention of cell death (79). Thus, it is possible that our detection of the α-tocopherol(hydro)quinones indicates the coral cells are frontloading the activated form of vitamin E, which is counteracting lipid peroxidation resulting in the detection of α-tocopherol(hydro)quinones.

When corals were previously challenged with bacterial pathogen-associated lipopolysaccharides, susceptible corals demonstrated a transcriptome response related to apoptosis, while resistant corals transcribed genes related to autophagy, a more modulated response to stressors (80). The damage threshold hypothesis proposes that coral disease susceptibility is inversely related to the upper limit of damage a coral can withstand before harmful effects are observed (81). Corals with a low damage threshold (high susceptibility) may be unable to modulate immune responses; either mounting too high of a response, leading to auto-immune challenges, or too low of a response before cellular death is imminent. Thus, the varied detection of tocopherol(hydro)quinones in this study should be further investigated to determine if these metabolites serve as a biomarker of corals particularly susceptible to disease, represent stressor history, and if they vary temporally with disease progression.

M. meandrites and *O. faveolata* had the highest relative abundance of α-tocomonoenol (Fig. 3A). α-Tocomonoenol was previously detected at higher abundance in apparently healthy *M. cavernosa* compared with diseased corals (43). The analog α-tocotrienol (*m/z* 424.333) with three degrees of unsaturation was exclusively detected in SCTLD-affected *M. cavernosa*, while other unsaturated analogs were likewise detected at higher abundance in the diseased corals (43). In this study, where we have analyzed healthy corals ahead of the SCTLD front, α-tocotrienol was not detected. Based on these results, we hypothesize that tocotrienols may serve as biomarkers for coral disease, wherein accumulation coincides with disease progression. A time course study that tracks how tocotrienol analogs and tocopherolquinones accumulate in response to disease exposure is required to validate this hypothesis. Recent work highlighting differential detection of tocopherol upon heat stress among resilient and susceptible species (48, 82) and our work reporting the detection of different tocopherol analogs among healthy and SCTLD-affected coral colonies suggest that this endosymbiont pathway likely plays an important role in coral health and resilience (48, 83); warranting studies that monitor tocopherol-related metabolite production over time after disease exposure.

Acylcarnitine profiles differentiate Meandrina meandrites

Feature 476.373_14.4 min was proposed by SIRIUS with CSI:FingerID as docosatetraenoyl carnitine (C22:4) (Fig. 4A and B). To confirm this annotation prediction and to determine if other acylcarnitines were present in our data, the output of the MS2LDA

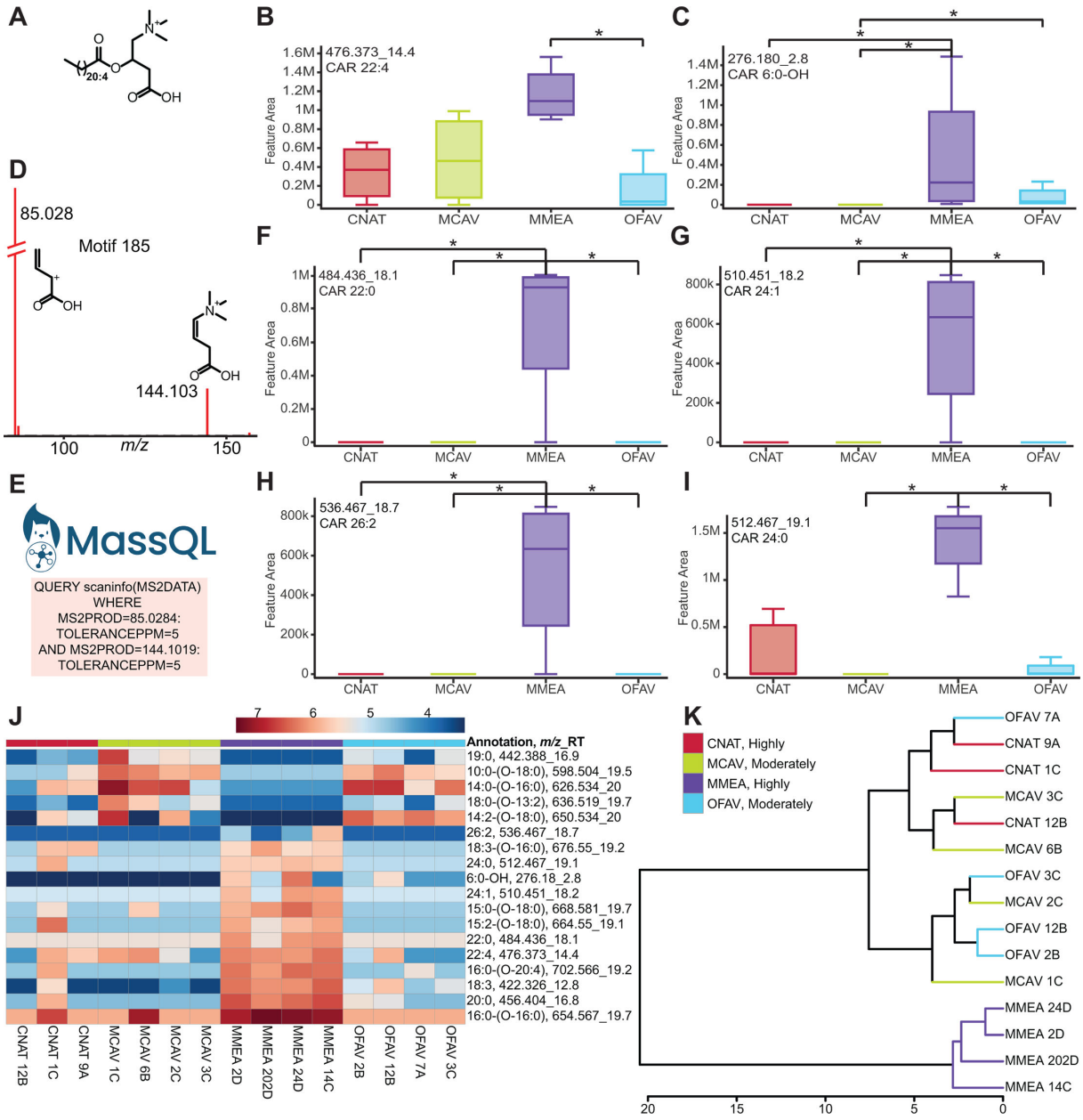

FIG 4 Annotation of and variation in detected acylcarnitines. (A) Chemical structure of docosatetraenoyl carnitine (C22:4). (B, C, F–I) A subset of the box plots of acylcarnitines differentially detected in the extracts of *M. meandrites*. Asterisks indicate significant differences as determined by a Kruskal Wallis test with Dunn's post-hoc test (adjusted $P < 0.05$). Additional box plots are reported in Fig. S4. (D) MS2LDA motif 185 used to aid annotations of features annotated as acylcarnitines. (E) The query submitted to MassQL to search for acylcarnitines. (J) Heat map of the features annotated as acylcarnitines that were determined as statistically differentiating by Kruskal Wallis test with Dunn's post-hoc test (adjusted $P < 0.05$). The scale bar represents the log-transformed abundance. The putative annotation and *m/z*_RT are included for each feature (Table S2; Fig. S5). (K) The hierarchical clustering analysis based on the log-transformed abundances of the acylcarnitines. The SCTLD susceptibility categorization is included in the key ("Highly," "Moderately").

analysis was consulted. This feature shares MS2LDA substructure motif 185 with feature 276.180_2.8 min, which was annotated as hydroxyhexanoyl carnitine (C6:0-OH) based on the MS^2 fragment peak at *m/z* 217.107 associated with the neutral loss of trimethylamine ($\Delta m/z$ = 59.07, Fig. 4C; S4A). A variety of acylcarnitines were further annotated with the aid of the GNPS spectral library, MassQL, substructure motif 185, and SIRIUS with CSI:FingerID (Fig. 4; Fig. S4B through O; Table S2).

Acylcarnitines are typically host-derived metabolites, and these metabolites were not detected in the cultured Symbiodiniaceae extracts in this study. Acylcarnitines have been detected at higher abundances in the daytime exometabolomes of *Porites* and *Pocillopora* compared to algae (turfing microalgae, macroalgae, and crustose coralline algae), where they are hypothesized to play a role in nitrogen and phosphorous cycling (84). Acylcarnitines play an integral role in metabolism of fatty acids in mitochondria (85) and maintenance of available pools of free coenzyme A (86). In the diatom *Phaeodactylum tricornutum*, propanoyl-carnitine and butanoyl-carnitine accumulate under nitrogen-starvation (87). Accumulation of acylcarnitine concentrations has been linked with cell toxicity (88), mitochondrial dysfunction (89–91), and dysfunction in cellular bioenergetics in humans (88). Acylcarnitines have been found to be upregulated in corals upon exposure to octocrylene, an ingredient used in sunscreens (51), which is the only study reporting conditional dysregulation of acylcarnitine levels in corals found in our literature search. In this study, the interspecies variation of all features annotated as acylcarnitines were analyzed with a Kruskal Wallis test with Dunn's post-test (adjusted $P < 0.05$). The acylcarnitines with fatty acyl tails with C13-C20 are classified as long chain, and tails > C21 as very long chain (92). Features that were differentially detected showed two interspecies patterns based on the acyl chain length (Fig. 4B, C and F through J; Fig. S4D through O). The hydroxyhexanoyl acylcarnitine and very long chain acylcarnitines were detected at a higher intensity in *M. meandrites* (Fig. 4B, C and F through I). The accumulation of long-chain acylcarnitines is associated with several metabolic diseases in humans (92). Differences in acylcarnitine profiles have also been reported as indicators of frailty in humans (93). Given that certain acylcarnitine analogs are detected at higher intensity in *M. meandrites* (Fig. 4; Fig. S4), a highly SCTLD-susceptible species, it is possible that acylcarnitine profiling could represent disease history and/or higher susceptibility to disease. Interestingly, when an HCA was performed on only the annotated acylcarnitine features, a clear separation of *M. meandrites* from other coral species was observed (Fig. 4K). Thus, host-derived acylcarnitines display a species-specific profile. Since several acylcarnitines were variably detected in these apparently healthy corals, the understudied role of carnitines in disease resilience and susceptibility in corals should be further investigated.

Several unknown acylcarnitines were distributed differentially across the coral species (Fig. 4J; Fig. S4G through O). Upon manual inspection of fragmentation spectra, we propose the annotation of these features as acylcarnitines containing fatty acid esters of hydroxy fatty acids (known as FAHFAs) (Fig. S5A; Table S2). The fragments at *m/z* 85.028 and 144.102, the presence of a fragment corresponding to hydroxylated fatty acid of acylcarnitine (CAR 14:1-OH), and the presence of an additional fatty acid tail fragment (C18:0) supported the annotation of an FAHFA-containing acylcarnitines [Fig. S5A, bottom spectrum; CAR 14:1-(O-18:0)]. FAHFAs are a conserved class of lipids that are widely reported, including in dietary plants (94, 95), as defense molecules in caterpillars named as mayolenes (96, 97), as anti-inflammatory metabolites in humans (98), and in the corallivore Crown-of-Thorns Starfish (99). Oxidative and environmental stress increase the synthesis of FAHFAs and ornithine-conjugated FAHFAs (100, 101). Acylcarnitines containing FAHFAs have not been previously reported and warrant further investigation for structural characterization and their role in coral biology. We searched for these acylcarnitines features in the publicly available data sets on the MassIVE server using MASST (102). These features were found in several marine organism-derived data sets including data sets from several coral species (Table S3) but were not observed in human-derived data sets. These observations further strengthen the role and application of modern methods in data analysis in untargeted metabolomics to discover biologically relevant metabolic pathways and generate testable hypotheses. Here, access to public data sets on these pristine endangered coral species is advantageous.

DGCC betaine lipids with 16:0 fatty acyl tails are differentially detected between species

Several differentiating features were identified as diacylglyceryl-carboxyhydroxymethylcholine (DGCC) betaine lipids. Feature 774.584_19.6 min was a GNPS library match to DGCC(36:5) (Fig. 5A; Fig. S6A). The fragment peaks at *m/z* 490.373 and 472.363 in the MS^2 spectra, which are characteristic of the chemical substructure containing a 16:0 fatty acyl tail, enable further annotation of this feature as DGCC(16:0_20:5) (Fig. S7). This feature was variably detected among coral species, present at the highest abundance in *M. cavernosa*. As expected, the feature 490.373_13.1 min, annotated as lyso-DGCC(16:0) known to be a constituent of healthy corals (43, 58, 103), was detected in all species (Fig. 5B; Fig. S6B). We used MassQL to search for additional DGCC analogs containing a 16:0 fatty acyl tail (Fig. S6C). This approach permitted the annotation of additional metabolite features, detected at highest abundances in *M. meandrites*, as lyso-DGCC(16:0) analogs (Fig. 5; Fig. S7; Table S2). Diacylated and unsaturated DGCC betaine lipids have been previously proposed as biomarkers of coral bleaching (58, 103). The increase in lipid unsaturation is suggestive of increased cell death when the antioxidative capacity of cells is lowered (104). DGCC betaine lipids are biosynthesized by Symbiodiniaceae (50). We searched the metabolite data acquired on cultured Symbiodiniaceae for the presence of the annotated DGCC analogs. While monoacylated lyso-DGCC(16:0) was detected in all cultured Symbiodiniaceae genera, the diacylated analogs were notably absent in *Durusdinium* extracts, the genera known to be most thermotolerant (105–108) (Fig. 5H). Roach et al. noted a higher abundance of lyso-DGCCs in historically non-bleached corals, while unsaturated and DGCCs were abundant in historically bleached corals (58). Rosset et al. observed significantly higher abundance of lyso-DGCC and unsaturated DGCCs in thermotolerant *D. trenchii* as compared to *Cladocopium* C3 in both control and heat-stressed conditions (49, 50). Symbiodiniaceae genera show differential responses to thermal and irradiance stress, which affects the entire holobiont response to stressors (64, 109–111). The variable detection of the DGCC(16:0) analogs in the coral extracts

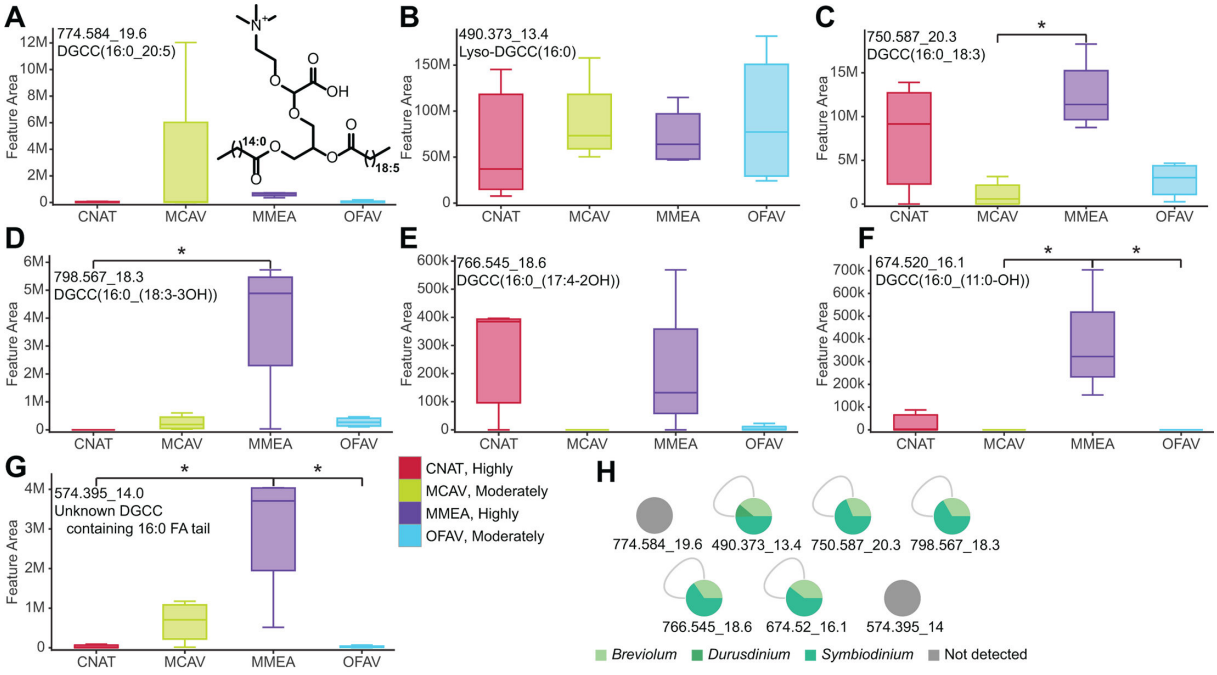

FIG 5 Interspecies variation of diacylglyceryl-carboxyhydroxymethylcholine (DGCC) betaine lipids. (A–G) Box plots of features annotated as DGCC(16:0) analogs. Annotations are provided in Fig. S6 and S7 and Table S2. Asterisks indicate significant differences between coral species as determined by Kruskal Wallis test with Dunn's post-hoc test (adjusted $P < 0.05$). (H) The detection pattern of DGCC analogs in the cultured zooxanthellae extracts. The SCTLD susceptibility categorization is included in the key ("Highly," "Moderately").

may indicate variable bleaching history or the presence or absence of certain Symbiodiniaceae species in the coral colonies sampled. Previous reports suggest that the DGCC lipid profile is influenced by the host (112). Given that algae transform their membranes in response to a variety of stimuli and stressors (113–115), it is also possible that the variable detection of the diacylated DGCC(16:0) analogs is reflective of host-dependent shifts in betaine lipid profiles of Symbiodiniaceae.

Carotenoid pigments do not show coral species-specific patterns

Carotenoids are important antioxidants in photosynthetic organisms. Symbiodiniaceae produce several carotenoids such as peridinin, fucoxanthin, astaxanthin, diatoxanthin, diadinoxanthin, and neoxanthin, with peridinin being the most prevalent and abundant (116, 117). We examined whether endosymbiont-derived pigment profiles contributed to variation among the coral colonies analyzed in this study. Several pigments were annotated using mass spectral search and literature search (Fig. 6; Fig. S8A through F; Table S2). The features annotated as pigments were also analyzed by HCA (Fig. 6B). The pigment profile did not display clear interspecies variation but did display intraspecies variation. Peridinin was detected in all coral extracts, while fucoxanthin was detected in only a few coral extracts (Fig. 6A). Among cultured Symbiodiniaceae in this study, peridinin was detected in all genera, whereas fucoxanthin was only detected in thermotolerant *Durusdinium* cultures (Fig. S8G). Since Wakahama et al. reported a negative correlation between the presence of fucoxanthin and peridinin in a variety of symbiotic and free living *Symbiodinium* strains (118), we confirmed the detection of fucoxanthin in peridinin-containing coral extracts using an analytical standard of fucoxanthin (Fig. S8F). The detection of both pigments may represent the presence of multiple strains of Symbiodiniaceae within the cultures.

Butanol partitions of whole coral extracts enable additional metabolite annotations

The crude extracts from the whole coral samples were further partitioned into ethyl acetate (EtOAc) and butanol (BuOH) solvents, and the bioactivity of these fractions was tested against the potential SCTLD-associated pathogens *Vibrio coralliilyticus* OfT6-21 and OfT7-21, *Leisingera* sp. McT4-56, and *Alteromonas* sp. McT4-15 (119, 120) using an agar disk-diffusion assay (Fig. 7A; Fig. S9A). Partitions only exhibited activity against *V. coralliilyticus* strains. The largest zones of inhibition were observed for BuOH partitions of *M. meandrites* against both pathogens (Fig. 7A; Fig. S9A). Thus, untargeted metabolomics data were acquired on BuOH partitions of all species. The metabolite data were analyzed following the scheme outlined in Fig. 1. Within the BuOH partitions, additional 560 metabolite features were detected (Fig. 7B). The UpSet Plot analysis showed the greatest number of unique features was detected in *C. natans* extracts, followed by *M. cavernosa*, *M. meandrites*, and *O. faveolata* (Fig. 7B). We used CANOPUS to predict the chemical classes of these features (Table S4). For the features uniquely detected in the BuOH partitions, none of the metabolites in the CANOPUS-predicted natural product pathways were significantly enriched in *M. meandrites* compared to the other species (Fig. 7C). The UpSet Plot and CANOPUS output were used to guide compound annotations (Fig. 7D).

A feature, detected exclusively in BuOH partitions at 280.157_7.9 min was annotated as Tau-C10:0 based on MS^2 spectral matching (Fig. S10A). We also observed the presence of the *N*-acyl taurines in several publicly available data sets acquired on diatoms, dinoflagellates, and seawater by searching the MS^2 spectrum of this metabolite in MASST (Table S3). *N*-acyl taurines have been implicated as important signaling molecules in several human processes including postprandial glucose regulation (121), but these molecules have not been previously described in corals. Thus, partitioning crude extracts into organic solvents can enable detection and characterization of low-abundance metabolites, which are otherwise below the limit of detection. Feature 267.960_5.3 min with an isotopic pattern of a brominated compound was uniquely detected in the

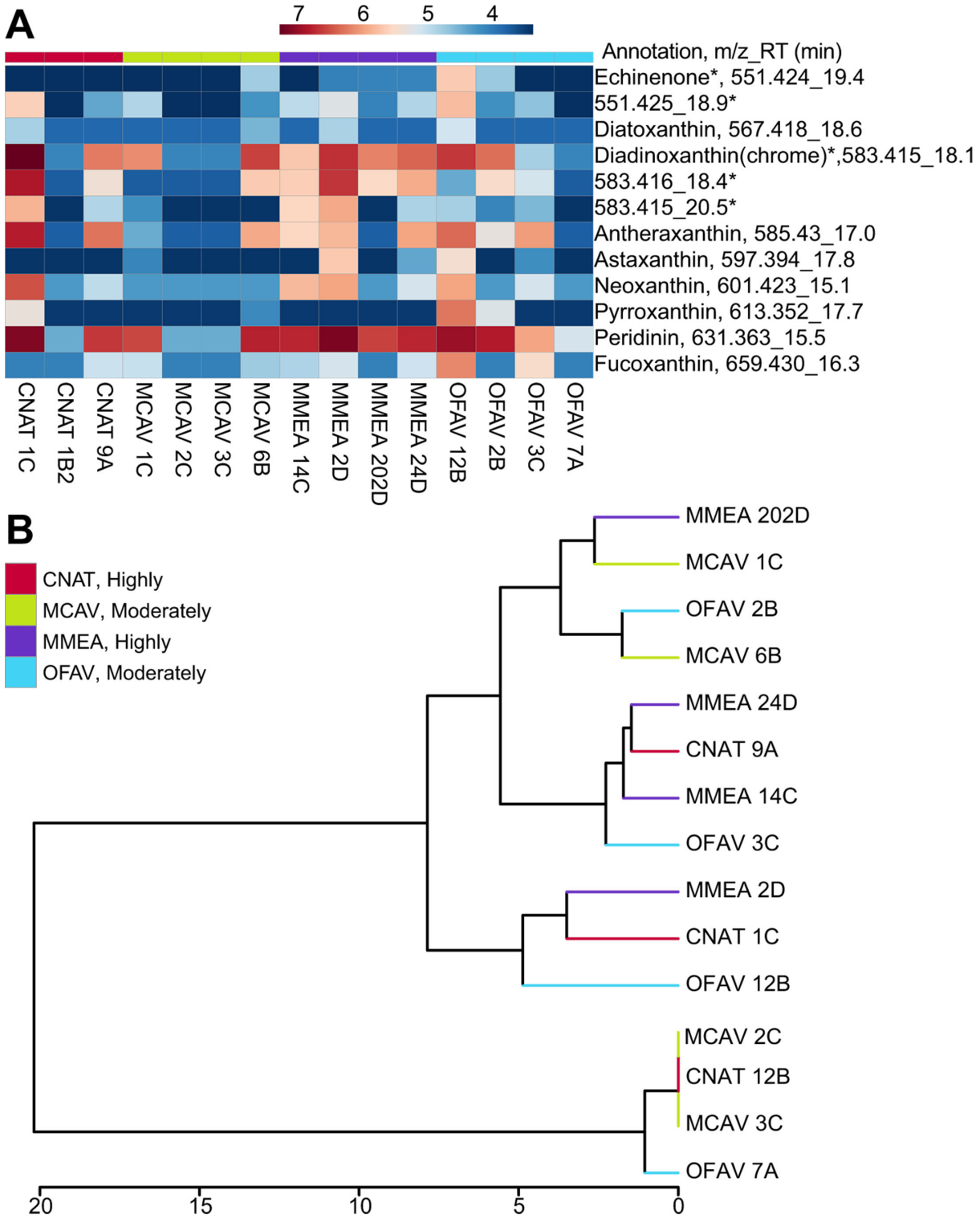

FIG 6 Analyses of endosymbiont-derived pigments. (A) Heat map showing the distribution of features annotated as pigments. The log-transformed abundance is reported. The *m/z*_RT and annotation are included. The * indicates these features have identical MS^2 spectra, but different retention times representing isomeric species. (B) Hierarchical clustering analysis based on the log-transformed abundance of the annotated pigments shows no clustering by species nor site. The SCTLD susceptibility categorization is included in the key ("Highly," "Moderately").

BuOH partitions of *O. faveolata*. This annotated as caelestine A based on MS^2 spectral matching and MS^1 isotopic pattern (Fig. S10B and C). CANOPUS predicted the chemical

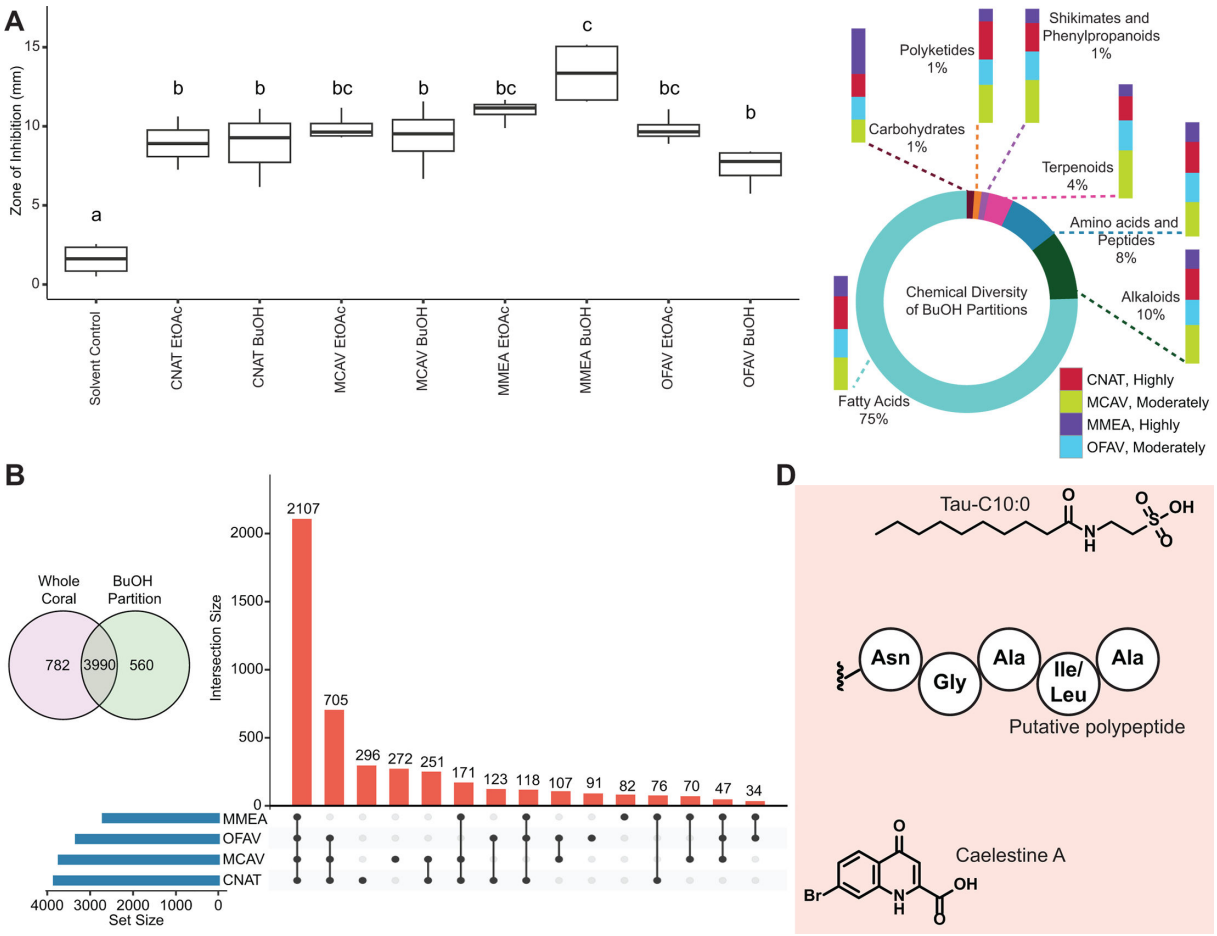

FIG 7 Analysis of BuOH partitions of crude extracts. (A) Bioactivity of EtOAc and BuOH partitions of crude extracts determined using agar diffusion growth inhibition assay against coral pathogen *V. coralliilyticus* OfT6-21. Letters denote results from a Tukey HSD posthoc test following a significant one-way ANOVA ($P < 0.001$). (B) Venn diagram of features detected in whole coral extracts and BuOH partitions. 560 unique metabolite features were detected in BuOH partitions. UpSet Plot of all features detected in BuOH partitions, where the number above each bar represents the number of features in that intersection and "Set Size" denotes the total number of features detected within that coral species. (MMEA = *M. meandrites*, OFAV = *O. faveolata*, MCAV = *M. cavernosa*, CNAT = *C. natans*). The SCTLD susceptibility categorization is included in the key ("Highly," "Moderately"). (C) Chemical diversity of features detected exclusively in BuOH partitions, along with the distribution of these features among the coral species. Natural product pathways (probability > 0.8) were determined using CANOPUS. (D) Chemical structures of putatively annotated metabolite features uniquely detected in BuOH partitions (annotations supported in Fig. S8 and S9).

class as hydropyrimidine carboxylic acids and derivatives. Caelestine A, a brominated quinoline carboxylic acid, has been reported as a possible indicator of a response to heat stress in the invasive bryozoan *Bugula neritina* (122). A feature at 615.346_5.9 min was proposed as a tunicyclin G analog by DEREPLICATOR, which compares experimental MS^2 spectra against predicted *in silico* MS^2 spectra of peptides (123) and CANOPUS predicted the chemical class of this feature as oligopeptides. We putatively annotated the feature 615.346_5.9 min as a polypeptide with partial sequence NGAI/LA (Fig. S9C). This polypeptide was detected in *M. cavernosa* and *O. faveolata* BuOH partitions. Although we could not link the enhanced antibacterial activity with specific molecules or chemical classes due to a small sample size, these annotations show that partitioning of whole coral metabolomic extracts increases the breadth of detected metabolites and enables annotation of low-abundance natural products. Annotation of individual metabolites is still a tedious and manual task. As spectral libraries are populated by the community, and *in silico* compound annotation methods advance, these data sets will be a valuable resource to untangle mechanisms of symbiosis between members of coral holobionts.

Conclusion

The visually healthy corals collected from the Dry Tortugas, a region of Florida with oceanographic conditions that support coral productivity, revealed interspecies metabolome differences. Tight clustering of the *M. meandrites* metabolome indicated similar metabolite profiles, while higher metabolome variation was found for *C. natans*, *M. cavernosa*, and *O. faveolata*. Metabolites driving the variation between species included tocopherol(hydro)quinones, diacylated betaine lipids, and acylcarnitines. This is the first report describing differences in acylcarnitine profiles between coral species and the discovery of potentially novel analogs containing an additional fatty acid group. Given the specificity of these acylcarnitine-FAHFA to only marine organisms based on the MASST search, the biochemical function of these molecules is of particular interest. The role of acylcarnitines in cellular energetics is well established; the varied detection of acylcarnitines in corals may indicate variability among species in their ability to readily utilize these pathways. Future work will focus on the structural description of these carnitines. How the profiles of metabolites reported in this paper change over time should also be characterized to determine their viability as biomarkers of health, disease, and lesion progression. The juxtaposition of *M. meandrites* SCTLD susceptibility and the observed highest bioactivity of the BuOH partitions of the extracts of this species against putative secondary SCTLD pathogens generates interesting avenues for future study, including how molecular dynamics of pathogen response and disease susceptibility might explain discrepancies between disease susceptibilities in the field while metabolite extracts show high antibacterial activity when challenged with in lab-assays to a specific pathogen. Additional studies can also incorporate knowledge of environmental factors like heat stress to determine how biochemical disease dynamics and susceptibility may shift in the field.

As SCTLD appears to affect Symbiodiniaceae and disrupt their relationship with the host (13, 38, 40, 43), it is imperative to understand the differences in chemical cross-talk between the corals and endosymbionts. Symbiodiniaceae dynamics within the host (e.g., relative abundance, density, species) will likely have an effect on the metabolomic profiles. In this study, several Symbiodiniaceae metabolites driving interspecies differences and endosymbiont-derived carotenoid pigments displayed both inter- and intraspecies variation suggesting the presence of different endosymbiont genotypes in these samples and/or different endosymbiont-host dynamics among species. Thus, metabolomic studies on Symbiodiniaceae directly isolated from field corals will enable source tracking to tease apart host-derived, diet-derived, and endosymbiont-derived compounds. Given that the endosymbiont fraction can be isolated from corals using mechanical methods such as the air brush technique (124), we propose future studies also include comprehensive metabolic profiling of these endosymbionts prior to and upon exposure to disease. Such differences should be interrogated across corals with different disease susceptibility and with different endosymbiont profiles. Furthermore, studies of metabolomic profiles taken at discrete time-points after disease exposure will provide insights into the transitory response of corals to disease stressors. With the increased application of untargeted metabolomics methods to study coral physiology, availability of annotated data sets, and our ability to mine public data sets using methods such as MASST, discoveries pertaining to chemical interactions between the coral host, the endosymbiont, environment, and the microbiome that define health status are a real possibility. By advancing our knowledge of the biochemical pathways involved in coral health and susceptibility to disease, we can disentangle the sources of metabolites, and how they change with time and increasing anthropogenic and climate-related stressors.

MATERIALS AND METHODS

Coral sample collection and extraction procedure

Whole coral fragments of a maximum size of 200 cm^2 were collected on SCUBA from four visually healthy Scleractinia coral species, *O. faveolata* (*n* = 4), *M. cavernosa* (*n* = 4), *M. meandrites* (*n* = 4), and *C. natans* (*n* = 3). These were collected in January 2020 from four sites outside of the Dry Tortugas National Park (Fig. 1; Table S1). This collection occurred ahead of the SCTLD front, which was first observed at the Dry Tortugas in May 2021 (125). Collection also occurred during a time of year when temperature stress and any associated paling or bleaching of the corals should not have been occurring, and none was observed at time of collection. Corals were chiseled at the base until they released from the substrate and then were transported back to the diving vessel in 18.9 L plastic bags filled with ocean water. Collected corals larger than 25 cm^2 were cut down to this size on the diving vessel using an AquaSaw (Gryphon C-40 CR). The cut portions and whole colonies were stored in a 1,000 L covered insulated container (Bonar Plastics, PB2145) filled halfway with ocean water. Air stones within the container allowed for aeration and water movement. A complete water change was performed on the container four times daily. Collections were conducted over 2 days before corals were transported the morning of the third day. The cruise was sponsored by the Florida Department of Environmental Protection and sample collection was covered by permit FKNMS-2019-160 to Valerie Paul. All corals collected from the field were transported to the Smithsonian Marine Station in Fort Pierce, FL. For transport, individual colonies were wrapped in plastic bubble wrap moistened with ocean water and then placed in a cooler.

Upon arrival, corals were rinsed with filtered seawater (FSW) and stored in a large indoor recirculating system holding approximately 570 L of FSW at 25.5°C ± 0.3°C. The FSW was collected from an intake pipe extending 1,600 m offshore South Hutchingson Island, Port Saint Lucie, FL and was filtered progressively through 20, 1.0, 0.5, and 0.35 µm pore filters. While stored prior to use in the recirculating system, the FSW constantly circulated through a 20-µm pore filter, a filter canister with ROX 0.8 aquarium carbon (Bulk Reef Supply), and a 36-watt Turbo-twist 12× UV sterilizer (Coralife) in series. The recirculating system contained a UV sterilizer (same model as described), two circulating pumps (AquaTop MaxFlow MCP-5) to create water movement, and a row of 6 blue-white 30 cm^2 LED panels (HQPR) to create 150–250 µmol photons m^{-2} s^{-1} for the captive corals. Corals were stored in the recirculating system for 5 days prior to sampling to allow them time to recover after transport, with a partial water change on the fourth day. All corals were held together in a single table.

After the 5th day, the corals were cut into smaller segments with a rock saw, and the blade was constantly sprayed down with UV/filter-sterilized seawater to cool the blade and wash off any debris, thus reducing cross-contamination between corals. The coral fragments ranged from 1 to 13 cm^2 in surface area (6.2 + 3.7 cm^2, mean + SD) were immediately frozen (−80°C) and lyophilized the next day. Coral fragments were lyophilized overnight and then extracted twice using a 2:2:1 mixture of ethyl acetate (EtOAc), methanol (MeOH) ,and water (H_2O) at room temperature in 20 mL scintillation vials. For the extraction, coral fragments were covered with an excess of solvent mixture, sonicated for 5–10 min and left to sit for 3 h on the initial extraction and overnight for the second extraction. The liquid extract was then transferred into a round-bottom flask using filter paper to prevent the transfer of coral fragments. The coral extract was then dried via rotary-evaporation (Buchi Rotovapor R-210) in a 35°C water bath (Buchi Heating Bath B-491) and weighed to determine the amount of crude extract. The extracts were dried *in vacuo* and 0.5 mg of the extract was transferred to Eppendorf tubes for metabolomics data analysis. The extracts were stored at −20°C until UPLC-MS data were acquired.

Endosymbiont metabolome data

We previously reported on metabolome profiles of Symbiodiniaceae isolates provided by Mary Alice Coffroth from the University of Buffalo Undersea Reef Research (BURR) collection (43). Given the challenges involved in isolating and culturing Symbiodiniaceae, we used this publicly available data (43) (MassIVE identifier MSV000087471) in this current study to aid in determining the biosynthetic producer of detected metabolites. Briefly, the endosymbionts were isolated by Mary Alice Coffroth from Orbicella faveolata corals sampled between 2002 and 2005 from the Florida Keys. Isolate extracts were sent by Richard Karp and Andrew Baker (University of Miami). Culture conditions included incubation at 27°C in F/2 media, with 20 µE of light on a 14:10 diurnal cycle. Extracts of the culture were performed as previously described (43), using 2:2:1 EtOAc:MeOH:H_2O to extract pelletized cellular cultures. Solvents were removed, and the dried samples were transferred in 3:1 MeOH:H_2O into a 1.5-mL microcentrifuge tube. After centrifugation, the supernatant was transferred to a microcentrifuge tube and removed via SpeedVac for 3 h. The extract was frozen, lyophilized, and analyzed using UPLC-MS/MS. Please see Deutsch et al. 2021 for detailed methodology (43).

Mass spectrometry data acquisition and analysis

The dried extracts were resuspended in 100% MeOH containing 1 µM sulfadimethoxine as an internal standard. The samples were analyzed with an Agilent 1290 Infinity II UHPLC system (Agilent Technologies) using a Kinetex 1.7 µm C18 reversed phase UHPLC column (50 × 2.1 mm) for chromatographic separation, coupled to an ImpactII ultra-high resolution Qq-TOF mass spectrometer (Bruker Daltonics, GmbH, Bremen, Germany) equipped with an ESI source for MS/MS analysis. MS/MS spectra were acquired in positive mode as previously described (43). Metabolomics data on the cultured Symbiodiniaceae from the Burr Collection were previously acquired (43). The strains utilized are reported in Table S5.

The raw data were converted to mzXML format using vendor software. MZmine 2.53 was used to extract metabolite features with steps for mass detection, chromatogram building, chromatogram deconvolution, isotopic grouping, retention time alignment, duplicate removal, and missing peak filling (126). These processed data were submitted to the feature-based molecular networking workflow on the Global Natural Product Social Molecular Networking (GNPS) platform (127). The output of MZmine includes information about LC-MS features across all samples containing the *m/z* value, retention time, the area under the peak for the corresponding chromatogram, and a unique identifier for each feature. The quantification table and the linked MS^2 spectra were exported using the GNPS export module (126, 128) and the SIRIUS 4.0 export module (126, 129). Feature Based Molecular Networking was performed using the MS^2 spectra (.mgf file) and the quantification table (.csv file). The molecular network was generated as previously described (43). The molecular network and the generation parameters are available here. The molecular network was visualized using Cytopscape v3.7.2 (130). The MS2LDA analysis was performed as previously described with default parameters (131, 132). The MassQL Sandbox Dashboard (133) (v 0.3) on the GNPS platform was used to construct the spectral pattern queries for the MassQL search. Feature annotation was performed using SIRIUS with CSI:FingerID, MolDiscovery (134), GNPS spectral library matching, MassQL, MASST, and literature searches. The metabolite annotations presented herein follow the "level 2" annotation standard based upon spectral similarity with public spectral libraries, spectra published in the literature, and through spectral comparison with the analytical standards as proposed by the Metabolomics Society Standard Initiative (135). All mzXML files included in this study can be accessed publicly on the repository Mass Spectrometry Interactive Virtual Environment (MassIVE) with ID MSV000089633. The commercial analytical standard for α-tocopherolquinone (catalog number 35365) was purchased from Cayman Chemical Company and the commercial analytical standard for fucoxanthin (catalog number 16337) was purchased from Sigma Aldrich.

Prior to statistical analysis, blank subtraction was performed as previously described (43) to filter out features detected in the solvent and media controls. Unsupervised multivariate statistical analyses including principal component analysis (136) and hierarchical clustering analysis (137) were performed using MetaboAnalyst 5.0 (138), and pareto scaling was employed prior to the analyses. The Plotter Dashboard (v.0.5) on the GNPS platform was used to construct boxplots for metabolite features of interest. A nonparametric Kruskal Wallis test with Dunn's posttest was performed in R studio. The UpSet Plots were made using the Intervene app (139).

To test for an effect of coral species on metabolomic variation, we used a permutational multivariate analysis of variance (PERMANOVA) (62). Coral species was treated as a fixed effect (four levels), with site included as a random nested effect (four levels). The PERMANOVA was based on a Bray-Curtis similarity matrix (140), type III (partial) sums of squares, and 999 random permutations of square-root transformed data (to down-weight heavily dominant variables) under a reduced model. Both PERMANOVA and non-metric multidimensional scaling (141) plot were constructed from a Bray-Curtis similarity matrix of square root transformed data, which was performed using PRIMER v7 (142). To quantify metabolomic variation within and between coral species, we calculated their multivariate dispersion using the PERMDISP routine (143). PERMDISP calculates the distance of each observation (in this case, each coral sample) to its group centroid (in this case, each coral species) and then compares the average of these distances among groups. It is a multivariate extension of Levene's test, with the *P*-values obtained using permutations of the raw data. This allowed us to make inferences about the relative size of the clouds in multivariate space within and between coral species. The tests were based on the same transformed data and Bray-Curtis similarity matrix as our PERMANOVA tests. Shannon entropy (144) was calculated for the alpha diversity metric using a Jupyter Notebook. A Bray-Curtis similarity matrix of log-transformed data was constructed using Primer v7 for the beta diversity metric. A principal coordinates analysis (145) was constructed on the Bray-Curtis similarity matrix.

Several *in silico* tools were used to aid in metabolite annotations. MolDiscovery compares *in silico* generated MS^2 spectra of small molecules to user-uploaded experimental MS^2 spectra (134). SIRIUS computes putative chemical formulas based on user-uploaded MS^1 isotopic peaks and MS^2 fragmentation patterns (129). CSI:FingerID transforms MS^2 spectra into predicted structural fingerprints that enable matching to fingerprints generated from structure databases (146). CANOPUS, which predicts the chemical class of metabolites by utilizing CSI:FingerID's predicted structural fingerprints, proposed the chemical class of 449.398_21.3 min as Vitamin E compounds (147). Unsupervised substructure discovery performed through MS2LDA (148) enabled annotations of several classes. Substructure motif 108 consisted of fragmentation peaks characteristic of tocopherol substructure (Fig. S3D). Motif 185 containing characteristic carnitine headgroup fragment peaks (91, 149) at *m/z* 85.028 and 144.102 (Fig. 4D) aided acylcarnitine annotations. Supervised substructure discovery was performed using MassQL, an MS query language platform that outputs metabolite features based on sets of user-defined fragment peaks and neutral losses (133).

Extract partitioning of crude extracts of coral metabolomes

Crude coral extracts were partitioned to remove salts and separate compounds based on polarity. First, 3 mL of EtOAc was added to 20 mL scintillation vials containing dry crude extracts. Vials were sonicated to resuspend the extracts for 30–60 s. Three milliliters of H_2O and another 1 mL of EtOAc was then added and the vials swirled to mix. Vials were then left to separate into distinct layers. The EtOAc layer was transferred via glass pipette into a clean and pre-weighed 20 mL scintillation vial. An additional 2 mL of EtOAC was then added to the crude mixture with water, swirled to mix, and left to separate again. The EtOAc layer was again transferred into the vial containing the EtOAc partition. The EtOAc partitions were then dried via a SpeedVac vacuum concentrator (Thermo Scientific Savant SPD121P) at 35°C. The remaining aqueous extract was then

partitioned using *n*-butanol (BuOH). Approximately 2 mL of BuOH was added to the aqueous extract, swirled to mix, and then left to sit until distinct layers formed. The BuOH partition was then transferred into a clean and pre-weighed 20 mL scintillation vial. Another round of BuOH partitioning was performed by adding an additional 1 mL of BuOH to the aqueous extract, mixing and allowing time for a final separation. The BuOH layer was transferred to the vial containing the initial BuOH partition, which was then dried via rotary-evaporation and analyzed using UPLC-HRMS. The BuOH partitions were resuspended, and LC-MS data were acquired and analyzed following the procedure outlined in "Mass spectrometry data acquisition and analysis," above.

Disk diffusion

Coral extracts were tested for antibacterial activity using disk diffusion growth inhibition assays against putative coral pathogens, *Vibrio coralliilyticus* OfT6-21 and *V. coralliilyticus* OfT7-21, *Leisingera* sp. McT4–56 and *Alteromonas* sp. McT4-15. To make pathogen lawns, overnight liquid cultures of pathogens were grown by inoculating 2–3 mL of seawater broth (4 g/L tryptone and 2 g/L yeast extract in 0.22 mm filtered seawater) with individual colonies of each strain and shaking culture tubes at 150 RPM and 28°C (Benchmark Incu-shaker 10LR). To coat seawater agar (seawater broth with 15 g/L agar) plates with a pathogen lawn, a 200 mL aliquot of liquid culture (OD600 = 0.5) was added to each plate (150 mm × 15 mm) and spread using sterile glass beads.

Coral partitions were tested by solubilizing partitions in MeOH to a concentration of 6.25 mg/mL and applying 4 µL aliquots to sterile paper disks (Whatman Grade 1) in triplicate (final amount 25 µg/disk). A filter disc with 4 µL of nalidixic acid at 15.62 mg/mL (62.5 µg) was used as a positive control. Negative controls were disks treated with MeOH only. Disks were given time to dry completely and then carefully transferred with sterile forceps to seawater agar plates containing freshly coated pathogen lawns. Disk diffusion plates were then incubated at 28°C overnight. After incubation, zones of inhibition (ZOI) were measured using digital calipers from the edge of the paper disk to the edge of the zone of bacterial growth inhibition.

ACKNOWLEDGMENTS

We thank Olivia Carmack for assistance collecting the corals in the Dry Tortugas and Woody Lee, Blake Ushijima, and Jay Houk for assistance cutting and caring for the corals in aquaria. We thank Monica Monge Loria for providing an image of cultured Symbiodiniaceae used in Fig. 1. We also thank the multi-agency effort funded by the Florida Department of Environmental Protection to collect corals. Healthy corals were collected for this study under Florida Keys National Marine Sanctuary Permit Number FKNMS-2019-160.

This study was supported by NSF CAREER award to N.G. (award number 2047235) and the Florida Department of Environmental Protection Office of Resilience and Coastal Protection-Southeast Region.

AUTHOR AFFILIATIONS

[1]School of Chemistry and Biochemistry, Engineered Biosystems Building, Center for Microbial Dynamics and Infection, Georgia Institute of Technology, Atlanta, Georgia, USA
[2]Smithsonian Marine Station, Smithsonian Institution, Fort Pierce, Florida, USA
[3]School of Ocean Sciences, Bangor University, Anglesey, United Kingdom
[4]GIS and Spatial Ecology Laboratory, Halmos College of Arts and Sciences, Nova Southeastern University, Dania Beach, Florida, USA

PRESENT ADDRESS

Neha Garg, 950 Atlantic Drive. Georgia Institute of Technology, Atlanta, Georgia, USA

AUTHOR ORCIDs

Jessica M. Deutsch http://orcid.org/0000-0002-4082-4536
Valerie J. Paul http://orcid.org/0000-0002-4691-1569
Neha Garg http://orcid.org/0000-0002-2760-7123

FUNDING

Funder	Grant(s)	Author(s)
National Science Foundation (NSF)	2047235	Neha Garg

DATA AVAILABILITY

The metabolomics data utilized in this study are available at gnps.ucsd.edu with MassIVE ID# MSV000089633. The data acquired in negative mode are also available in this data set, but are not presented in this study due to the lack of high-confidence annotations. The code utilized in this study is available at https://github.com/Garg-Lab/Dry-Tortugas-Corals-Files.

ETHICS APPROVAL

The sample collection was covered by permit FKNMS-2019-160 to Valerie J. Paul.

ADDITIONAL FILES

The following material is available online.

Supplemental Material

Supplemental Figures and Tables (mSystems00856-24-S0001.docx). Fig. S1-S10; Tables S1-S5.

REFERENCES

1. Plaisance L, Caley MJ, Brainard RE, Knowlton N. 2011. The diversity of coral reefs: what are we missing? PLoS One 6:e25026. https://doi.org/10.1371/journal.pone.0025026
2. Fisher R, O'Leary RA, Low-Choy S, Mengersen K, Knowlton N, Brainard RE, Caley MJ. 2015. Species richness on coral reefs and the pursuit of convergent global estimates. Curr Biol 25:500–505. https://doi.org/10.1016/j.cub.2014.12.022
3. Brander L, Beukering P. 2013. The total economic value of U.S. coral reefs: a review of the literature, p 1–32. Silver Spring, MD.
4. Reguero BG, Storlazzi CD, Gibbs AE, Shope JB, Cole AD, Cumming KA, Beck MW. 2021. The value of US coral reefs for flood risk reduction. Nat Sustain 4:688–698. https://doi.org/10.1038/s41893-021-00706-6
5. Woodhead AJ, Hicks CC, Norström AV, Williams GJ, Graham NAJ. 2019. Coral reef ecosystem services in the Anthropocene. Funct Ecol 33:1023–1034. https://doi.org/10.1111/1365-2435.13331
6. Weil E, Rogers CS. 2011. Coral reef diseases in the Atlantic-Caribbean, p 465–491. In Dubinsky Z, Stambler N (ed), Coral reefs: an ecosystem in transition. Springer Netherlands, Dordrecht.
7. Montilla LM, Ascanio A, Verde A, Croquer A. 2019. Systematic review and meta-analysis of 50 years of coral disease research visualized through the scope of network theory. PeerJ 7:e7041. https://doi.org/10.7717/peerj.7041
8. Richardson LL. 1998. Coral diseases: what is really known? Trends Ecol Evol (Amst) 13:438–443. https://doi.org/10.1016/S0169--5347(98)01460-8
9. Rosenberg E, Ben-Haim Y. 2002. Microbial diseases of corals and global warming. Environ Microbiol 4:318–326. https://doi.org/10.1046/j.1462-2920.2002.00302.x
10. Neely KL, Lewis CL, Lunz KS, Kabay L. 2021. Rapid population decline of the pillar coral *Dendrogyra cylindrus* along the Florida Reef Tract. Front Mar Sci 8:656515. https://doi.org/10.3389/fmars.2021.656515
11. Precht WF, Gintert BE, Robbart ML, Fura R, van Woesik R. 2016. Unprecedented disease-related coral mortality in southeastern Florida. Sci Rep 6:31374. https://doi.org/10.1038/srep31374
12. Kramer PR, Roth L, Lang J. 2020. Caribbean SCTLD dashboard. ArcGIS Online. Available from: www.agrra.org
13. Aeby GS, Ushijima B, Campbell JE, Jones S, Williams GJ, Meyer JL, Häse C, Paul VJ. 2019. Pathogenesis of a tissue loss disease affecting multiple species of corals along the Florida Reef Tract. Front Mar Sci 6:678. https://doi.org/10.3389/fmars.2019.00678
14. Meiling SS, Muller EM, Lasseigne D, Rossin A, Veglia AJ, MacKnight N, Dimos B, Huntley N, Correa AMS, Smith TB, Holstein DM, Mydlarz LD, Apprill A, Brandt ME. 2021. Variable species responses to experimental Stony Coral Tissue Loss Disease (SCTLD) exposure. Front Mar Sci 8:670829. https://doi.org/10.3389/fmars.2021.670829
15. FDEP. 2018. Final report: stony coral tissue loss disease (SCTLD) case definition. Florida Department of Enviornmental Protection
16. Papke E, Carreiro A, Dennison C, Deutsch JM, Isma LM, Meiling SS, Rossin AM, Baker AC, Brandt ME, Garg N, Holstein DM, Traylor-Knowles N, Voss JD, Ushijima B. 2024. Stony coral tissue loss disease: a review of emergence, impacts, etiology, diagnostics, and intervention. Front Mar Sci 10:10. https://doi.org/10.3389/fmars.2023.1321271
17. Rohwer F, Seguritan V, Azam F, Knowlton N. 2002. Diversity and distribution of coral-associated bacteria. Mar Ecol Prog Ser 243:1–10. https://doi.org/10.3354/meps243001
18. Ainsworth TD, Fordyce AJ, Camp EF. 2017. The other microeukaryotes of the coral reef microbiome. Trends Microbiol 25:980–991. https://doi.org/10.1016/j.tim.2017.06.007
19. Blackall LL, Wilson B, van Oppen MJH. 2015. Coral—the world's most diverse symbiotic ecosystem. Mol Ecol 24:5330–5347. https://doi.org/10.1111/mec.13400

20. Bourne DG, Garren M, Work TM, Rosenberg E, Smith GW, Harvell CD. 2009. Microbial disease and the coral holobiont. Trends Microbiol 17:554–562. https://doi.org/10.1016/j.tim.2009.09.004
21. Muscatine L. 1990. Edited by DubinskyZ. The role of symbiotic algae in carbon and energy flux in reef corals. Vol. 25. Elsevier Science, Amsterdam.
22. LaJeunesse TC, Parkinson JE, Gabrielson PW, Jeong HJ, Reimer JD, Voolstra CR, Santos SR. 2018. Systematic revision of Symbiodiniaceae highlights the antiquity and diversity of coral endosymbionts. Curr Biol 28:2570–2580. https://doi.org/10.1016/j.cub.2018.07.008
23. Maire J, Girvan SK, Barkla SE, Perez-Gonzalez A, Suggett DJ, Blackall LL, van Oppen MJH. 2021. Intracellular bacteria are common and taxonomically diverse in cultured and in hospite algal endosymbionts of coral reefs. ISME J 15:2028–2042. https://doi.org/10.1038/s41396-021-00902-4
24. Pogoreutz C, Oakley CA, Rädecker N, Cárdenas A, Perna G, Xiang N, Peng L, Davy SK, Ngugi DK, Voolstra CR. 2022. Coral holobiont cues prime *Endozoicomonas* for a symbiotic lifestyle. ISME J 16:1883–1895. https://doi.org/10.1038/s41396-022-01226-7
25. Pollock FJ, McMinds R, Smith S, Bourne DG, Willis BL, Medina M, Thurber RV, Zaneveld JR. 2018. Coral-associated bacteria demonstrate phylosymbiosis and cophylogeny. Nat Commun 9:4921. https://doi.org/10.1038/s41467-018-07275-x
26. Cunning R, Baker AC. 2013. Excess algal symbionts increase the susceptibility of reef corals to bleaching. Nat Clim Change 3:259–262. https://doi.org/10.1038/nclimate1711
27. Sampayo EM, Ridgway T, Bongaerts P, Hoegh-Guldberg O. 2008. Bleaching susceptibility and mortality of corals are determined by fine-scale differences in symbiont type. Proc Natl Acad Sci U S A 105:10444–10449. https://doi.org/10.1073/pnas.0708049105
28. Klein AM, Sturm AB, Eckert RJ, Walker BK, Neely KL, Voss JD. 2024. Algal symbiont genera but not coral host genotypes correlate to stony coral tissue loss disease susceptibility among *Orbicella faveolata* colonies in South Florida. Front Mar Sci 11:1287457. https://doi.org/10.3389/fmars.2024.1287457
29. Matthews JL, Khalil A, Siboni N, Bougoure J, Guagliardo P, Kuzhiumparambil U, DeMaere M, Le Reun NM, Seymour JR, Suggett DJ, Raina J-B. 2023. Coral endosymbiont growth is enhanced by metabolic interactions with bacteria. Nat Commun 14:6864. https://doi.org/10.1038/s41467-023-42663-y
30. Reshef L, Koren O, Loya Y, Zilber-Rosenberg I, Rosenberg E. 2006. The coral probiotic hypothesis. Environ Microbiol 8:2068–2073. https://doi.org/10.1111/j.1462-2920.2006.01148.x
31. Pogoreutz C, Voolstra CR, Rädecker N, Weis V, Cárdenas A, Raina J-B. 2020. The coral holobiont highlights the dependence of cnidarian animal hosts on their associated microbes, p 91–118. In Cellular dialogues in the Holobiont. CRC Press.
32. Silverstein RN, Cunning R, Baker AC. 2015. Change in algal symbiont communities after bleaching, not prior heat exposure, increases heat tolerance of reef corals. Glob Chang Biol 21:236–249. https://doi.org/10.1111/gcb.12706
33. Manzello DP, Matz MV, Enochs IC, Valentino L, Carlton RD, Kolodziej G, Serrano X, Towle EK, Jankulak M. 2019. Role of host genetics and heat-tolerant algal symbionts in sustaining populations of the endangered coral *Orbicella faveolata* in the Florida Keys with ocean warming. Glob Chang Biol 25:1016–1031. https://doi.org/10.1111/gcb.14545
34. Palacio-Castro AM, Smith TB, Brandtneris V, Snyder GA, van Hooidonk R, Maté JL, Manzello D, Glynn PW, Fong P, Baker AC. 2023. Increased dominance of heat-tolerant symbionts creates resilient coral reefs in near-term ocean warming. Proc Natl Acad Sci U S A 120:e2202388120. https://doi.org/10.1073/pnas.2202388120
35. Quigley KM, Randall CJ, van Oppen MJH, Bay LK. 2020. Assessing the role of historical temperature regime and algal symbionts on the heat tolerance of coral juveniles. Biol Open 9:bio047316. https://doi.org/10.1242/bio.047316
36. Buerger P, Alvarez-Roa C, Coppin CW, Pearce SL, Chakravarti LJ, Oakeshott JG, Edwards OR, van Oppen MJH. 2020. Heat-evolved microalgal symbionts increase coral bleaching tolerance. Sci Adv 6:eaba2498. https://doi.org/10.1126/sciadv.aba2498
37. Grottoli AG, Rodrigues LJ, Palardy JE. 2006. Heterotrophic plasticity and resilience in bleached corals. Nature 440:1186–1189. https://doi.org/10.1038/nature04565
38. Landsberg JH, Kiryu Y, Peters EC, Wilson PW, Perry N, Waters Y, Maxwell KE, Huebner LK, Work TM. 2020. Stony coral tissue loss disease in Florida is associated with disruption of host–zooxanthellae physiology. Front Mar Sci 7:576013. https://doi.org/10.3389/fmars.2020.576013
39. Beavers KM, Van Buren EW, Rossin AM, Emery MA, Veglia AJ, Karrick CE, MacKnight NJ, Dimos BA, Meiling SS, Smith TB, Apprill A, Muller EM, Holstein DM, Correa AMS, Brandt ME, Mydlarz LD. 2023. Stony coral tissue loss disease induces transcriptional signatures of *in situ* degradation of dysfunctional Symbiodiniaceae. Nat Commun 14:2915. https://doi.org/10.1038/s41467-023-38612-4
40. Work TM, Weatherby TM, Landsberg JH, Kiryu Y, Cook SM, Peters EC. 2021. Viral-like particles are associated with endosymbiont pathology in Florida corals affected by stony coral tissue loss disease. Front Mar Sci 8:750658. https://doi.org/10.3389/fmars.2021.750658
41. Traylor-Knowles N, Baker AC, Beavers KM, Garg N, Guyon JR, Hawthorn A, MacKnight NJ, Medina M, Mydlarz LD, Peters EC, Stewart JM, Studivan MS, Voss JD. 2022. Advances in coral immunity 'omics in response to disease outbreaks. Front Mar Sci 9:952199. https://doi.org/10.3389/fmars.2022.952199
42. Barshis DJ, Ladner JT, Oliver TA, Seneca FO, Traylor-Knowles N, Palumbi SR. 2013. Genomic basis for coral resilience to climate change. Proc Natl Acad Sci U S A 110:1387–1392. https://doi.org/10.1073/pnas.1210224110
43. Deutsch JM, Jaiyesimi OA, Pitts KA, Houk J, Ushijima B, Walker BK, Paul VJ, Garg N. 2021. Metabolomics of healthy and stony coral tissue loss disease affected *Montastraea cavernosa* corals. Front Mar Sci 8:714778. https://doi.org/10.3389/fmars.2021.714778
44. Garg N. 2021. Metabolomics in functional interrogation of individual holobiont members. mSystems 6:e0084121. https://doi.org/10.1128/mSystems.00841-21
45. Lohr KE, Khattri RB, Guingab-Cagmat J, Camp EF, Merritt ME, Garrett TJ, Patterson JT. 2019. Metabolomic profiles differ among unique genotypes of a threatened Caribbean coral. Sci Rep 9:6067. https://doi.org/10.1038/s41598-019-42434-0
46. Becker CC, Weber L, Zgliczynski B, Sullivan C, Sandin S, Muller E, Clark AS, Kido Soule MC, Longnecker K, Kujawinski EB, Apprill A. 2023. Microorganisms and dissolved metabolites distinguish Florida's Coral Reef habitats. PNAS Nexus 2:pgad287. https://doi.org/10.1093/pnasnexus/pgad287
47. Oliveira JAS, Pereira RC, Nocchi N, Soares AR. 2022. Spatio-temporal variability of secondary metabolites in the invasive coral *Tubastraea coccinea*. Aquat Invasions 17:476–493. https://doi.org/10.3391/ai.2022.17.4.02
48. Haydon TD, Matthews JL, Seymour JR, Raina J-B, Seymour JE, Chartrand K, Camp EF, Suggett DJ. 2023. Metabolomic signatures of corals thriving across extreme reef habitats reveal strategies of heat stress tolerance. Proc Biol Sci 290:20221877. https://doi.org/10.1098/rspb.2022.1877
49. Leblond JD, Khadka M, Duong L, Dahmen JL. 2015. Squishy lipids: temperature effects on the betaine and galactolipid profiles of a C_{18}/C_{18} peridinin-containing dinoflagellate, *Symbiodinium microadriaticum* (Dinophyceae), isolated from the mangrove jellyfish, *Cassiopea xamachana*. Phycol Res 63:219–230. https://doi.org/10.1111/pre.12093
50. Rosset S, Koster G, Brandsma J, Hunt AN, Postle AD, D'Angelo C. 2019. Lipidome analysis of *Symbiodiniaceae* reveals possible mechanisms of heat stress tolerance in reef coral symbionts. Coral Reefs 38:1241–1253. https://doi.org/10.1007/s00338-019-01865-x
51. Stien D, Clergeaud F, Rodrigues AMS, Lebaron K, Pillot R, Romans P, Fagervold S, Lebaron P. 2019. Metabolomics reveal that octocrylene accumulates in *Pocillopora damicornis* tissues as fatty acid conjugates and triggers coral cell mitochondrial dysfunction. Anal Chem 91:990–995. https://doi.org/10.1021/acs.analchem.8b04187
52. Stony coral tissue loss on Florida's Coral Reef. 2022. Available from: https://www.nps.gov/drto/learn/nature/stony-coral-tissue-loss-on-florida-s-coral-reef.htm. Retrieved 15 Feb 2022.
53. Williamson OM, Dennison CE, O'Neil KL, Baker AC. 2022. Susceptibility of Caribbean brain coral recruits to Stony Coral Tissue Loss Disease (SCTLD). Front Mar Sci 9:9. https://doi.org/10.3389/fmars.2022.821165

54. Chapron L, Kuffner IB, Kemp DW, Hulver AM, Keister EF, Stathakopoulos A, Bartlett LA, Lyons EO, Grottoli AG. 2023. Heterotrophy, microbiome, and location effects on restoration efficacy of the threatened coral *Acropora palmata*. Commun Earth Environ 4:233. https://doi.org/10.1038/s43247-023-00888-1
55. Kuffner IB, Hickey TD, Morrison JM. 2013. Calcification rates of the massive coral *Siderastrea siderea* and crustose coralline algae along the Florida Keys (USA) outer-reef tract. Coral Reefs 32:987–997. https://doi.org/10.1007/s00338-013-1047-8
56. Lenz EA, Bartlett LA, Stathakopoulos A, Kuffner IB. 2021. Physiological differences in bleaching response of the coral *Porites astreoides* along the Florida Keys Reef Tract during high-temperature stress. Front Mar Sci 8:615795. https://doi.org/10.3389/fmars.2021.615795
57. Henry JA, Khattri RB, Guingab-Cagmat J, Merritt ME, Garrett TJ, Patterson JT, Lohr KE. 2021. Intraspecific variation in polar and nonpolar metabolite profiles of a threatened Caribbean coral. Metabolomics (Los Angel) 17:60. https://doi.org/10.1007/s11306-021-01808-0
58. Roach TNF, Dilworth J, H CM, Jones AD, Quinn RA, Drury C. 2021. Metabolomic signatures of coral bleaching history. Nat Ecol Evol 5:495–503. https://doi.org/10.1038/s41559-020-01388-7
59. Roach TNF, Little M, Arts MGI, Huckeba J, Haas AF, George EE, Quinn RA, Cobián-Güemes AG, Naliboff DS, Silveira CB, Vermeij MJA, Kelly LW, Dorrestein PC, Rohwer F. 2020. A multiomic analysis of *in situ* coral–turf algal interactions. Proc Natl Acad Sci U S A 117:13588–13595. https://doi.org/10.1073/pnas.1915455117
60. Little M, George EE, Arts MGI, Shivak J, Benler S, Huckeba J, Quinlan ZA, Boscaro V, Mueller B, Güemes AGC, Rojas MI, White B, Petras D, Silveira CB, Haas AF, Kelly LW, Vermeij MJA, Quinn RA, Keeling PJ, Dorrestein PC, Rohwer F, Roach TNF. 2021. Three-dimensional molecular cartography of the caribbean reef-building coral *Orbicella faveolata*. Front Mar Sci 8:8. https://doi.org/10.3389/fmars.2021.627724
61. Sogin EM, Putnam HM, Anderson PE, Gates RD. 2016. Metabolomic signatures of increases in temperature and ocean acidification from the reef-building coral, *Pocillopora damicornis*. Metabolomics12:71. https://doi.org/10.1007/s11306-016-0987-8
62. Anderson MJ. 2001. A new method for non-parametric multivariate analysis of variance. Austral Ecol 26:32–46. https://doi.org/10.1111/j.1442-9993.2001.01070.pp.x
63. Vohsen SA, Fisher CR, Baums IB. 2019. Metabolomic richness and fingerprints of deep-sea coral species and populations. Metabolomics15:34. https://doi.org/10.1007/s11306-019-1500-y
64. Baker AC. 2003. Flexibility and specificity in coral-algal symbiosis: diversity, ecology, and biogeography of *Symbiodinium*. Annu Rev Ecol Evol Syst 34:661–689. https://doi.org/10.1146/annurev.ecolsys.34.011802.132417
65. Roth MS. 2014. The engine of the reef: photobiology of the coral–algal symbiosis. Front Microbiol 5:422. https://doi.org/10.3389/fmicb.2014.00422
66. Klueter A, Crandall JB, Archer FI, Teece MA, Coffroth MA. 2015. Taxonomic and environmental variation of metabolite profiles in marine dinoflagellates of the genus *Symbiodinium*. Metabolites 5:74–99. https://doi.org/10.3390/metabo5010074
67. Grupstra CGB, Gómez-Corrales M, Fifer JE, Aichelman HE, Meyer-Kaiser KS, Prada C, Davies SW. 2024. Integrating cryptic diversity into coral evolution, symbiosis and conservation. Nat Ecol Evol 8:622–636. https://doi.org/10.1038/s41559-023-02319-y
68. Serrano X, Baums IB, O'Reilly K, Smith TB, Jones RJ, Shearer TL, Nunes FLD, Baker AC. 2014. Geographic differences in vertical connectivity in the Caribbean coral *Montastraea cavernosa* despite high levels of horizontal connectivity at shallow depths. Mol Ecol 23:4226–4240. https://doi.org/10.1111/mec.12861
69. Rippe JP, Dixon G, Fuller ZL, Liao Y, Matz M. 2021. Environmental specialization and cryptic genetic divergence in two massive coral species from the Florida Keys Reef Tract. Mol Ecol 30:3468–3484. https://doi.org/10.1111/mec.15931
70. Gómez-Corrales M, Prada C. 2020. Cryptic lineages respond differently to coral bleaching. Mol Ecol 29:4265–4273. https://doi.org/10.1111/mec.15631
71. Weil E, Knowton N. 1994. A multi-character analysis of the Caribbean coral *Montastraea annularis* (Ellis and Solander, 1786) and its two sibling species, *M. faveolata* (Ellis and Solander, 1786) and *M. franksi* (Gregory, 1895). Bull Mar Sci 55:151–175.
72. Mottier P, Gremaud E, Guy PA, Turesky RJ. 2002. Comparison of gas chromatography-mass spectrometry and liquid chromatography-tandem mass spectrometry methods to quantify alpha-tocopherol and alpha-tocopherolquinone levels in human plasma. Anal Biochem 301:128–135. https://doi.org/10.1006/abio.2001.5486
73. Siegel D, Bolton EM, Burr JA, Liebler DC, Ross D. 1997. The reduction of alpha-tocopherolquinone by human NAD(P)H: quinone oxidoreductase: the role of alpha-tocopherolhydroquinone as a cellular antioxidant. Mol Pharmacol 52:300–305. https://doi.org/10.1124/mol.52.2.300
74. Takaaki H, Akio K, Masao N, Mamoru T, Hharuhisa S. 1992. Reduction of α-tocopherolquinone to α-tocopherolhydroquinone in rat hepatocytes. Biochem Pharmacol 44:489–493. https://doi.org/10.1016/0006-2952(92)90440-T
75. van der Hooft JJJ, Wandy J, Barrett MP, Burgess KEV, Rogers S. 2016. Topic modeling for untargeted substructure exploration in metabolomics. Proc Natl Acad Sci USA 113:13738–13743. https://doi.org/10.1073/pnas.1608041113
76. Murphy ME, Kolvenbach R, Aleksis M, Hansen R, Sies H. 1992. Antioxidant depletion in aortic crossclamping ischemia: increase of the plasma α-tocopheryl quinone/α-tocopherol ratio. Free Rad Biol Med 13:95–100. https://doi.org/10.1016/0891-5849(92)90069-S
77. Terentis AC, Thomas SR, Burr JA, Liebler DC, Stocker R. 2002. Vitamin E oxidation in human atherosclerotic lesions. Circ Res 90:333–339. https://doi.org/10.1161/hh0302.104454
78. Gaschler MM, Stockwell BR. 2017. Lipid peroxidation in cell death. Biochem Biophys Res Commun 482:419–425. https://doi.org/10.1016/j.bbrc.2016.10.086
79. Hinman A, Holst CR, Latham JC, Bruegger JJ, Ulas G, McCusker KP, Amagata A, Davis D, Hoff KG, Kahn-Kirby AH, Kim V, Kosaka Y, Lee E, Malone SA, Mei JJ, Richards SJ, Rivera V, Miller G, Trimmer JK, Shrader WD. 2018. Vitamin E hydroquinone is an endogenous regulator of ferroptosis via redox control of 15-lipoxygenase. PLoS One 13:e0201369. https://doi.org/10.1371/journal.pone.0201369
80. Fuess LE, Pinzón C JH, Weil E, Grinshpon RD, Mydlarz LD. 2017. Life or death: disease-tolerant coral species activate autophagy following immune challenge. Proc R Soc B 284:20170771. https://doi.org/10.1098/rspb.2017.0771
81. Palmer CV. 2018. Immunity and the coral crisis. Commun Biol 1:91. https://doi.org/10.1038/s42003-018-0097-4
82. Hillyer KE, Dias DA, Lutz A, Wilkinson SP, Roessner U, Davy SK. 2017. Metabolite profiling of symbiont and host during thermal stress and bleaching in the coral *Acropora aspera*. Coral Reefs 36:105–118. https://doi.org/10.1007/s00338-016-1508-y
83. Mesa T, Munné-Bosch S. 2023. α-Tocopherol in chloroplasts: nothing more than an antioxidant? Curr Opin Plant Biol 74:102400. https://doi.org/10.1016/j.pbi.2023.102400
84. Wegley Kelly L, Nelson CE, Petras D, Koester I, Quinlan ZA, Arts MGI, Nothias L-F, Comstock J, White BM, Hopmans EC, van Duyl FC, Carlson CA, Aluwihare LI, Dorrestein PC, Haas AF. 2022. Distinguishing the molecular diversity, nutrient content, and energetic potential of exometabolomes produced by macroalgae and reef-building corals. Proc Natl Acad Sci U S A 119:e2110283119. https://doi.org/10.1073/pnas.2110283119
85. Rebouche CJ, Seim H. 1998. Carnitine metabolism and its regulation in microorganisms and mammals. Annu Rev Nutr 18:39–61. https://doi.org/10.1146/annurev.nutr.18.1.39
86. Indiveri C, Iacobazzi V, Tonazzi A, Giangregorio N, Infantino V, Convertini P, Console L, Palmieri F. 2011. The mitochondrial carnitine/acylcarnitine carrier: function, structure and physiopathology. Mol Aspects Med 32:223–233. https://doi.org/10.1016/j.mam.2011.10.008
87. Popko J, Herrfurth C, Feussner K, Ischebeck T, Iven T, Haslam R, Hamilton M, Sayanova O, Napier J, Khozin-Goldberg I, Feussner I. 2016. Metabolome analysis reveals betaine lipids as major source for triglyceride formation, and the accumulation of sedoheptulose during nitrogen-starvation of *Phaeodactylum tricornutum*. PLoS One 11:e0164673. https://doi.org/10.1371/journal.pone.0164673
88. McCoin CS, Knotts TA, Ono-Moore KD, Oort PJ, Adams SH. 2015. Long-chain acylcarnitines activate cell stress and myokine release in C_2C_{12} myotubes: calcium-dependent and -independent effects. Am J Physiol

Endocrinol Metab 308:E990–E1000. https://doi.org/10.1152/ajpendo.00602.2014
89. Siliprandi D, Biban C, Testa S, Toninello A, Siliprandi N. 1992. Effects of palmitoyl CoA and palmitoyl carnitine on the membrane potential and Mg^{2+} content of rat heart mitochondria. Mol Cell Biochem 116:117–123. https://doi.org/10.1007/978-1-4615-3514-0_17
90. Tominaga H, Katoh H, Odagiri K, Takeuchi Y, Kawashima H, Saotome M, Urushida T, Satoh H, Hayashi H. 2008. Different effects of palmitoyl-L-carnitine and palmitoyl-CoA on mitochondrial function in rat ventricular myocytes. Am J Physiol Heart Circ Physiol 295:H105–H112. https://doi.org/10.1152/ajpheart.01307.2007
91. Vissing CR, Dunø M, Wibrand F, Christensen M, Vissing J. 2019. Hydroxylated long-chain acylcarnitines are biomarkers of mitochondrial myopathy. J Clin Endocrinol Metab 104:5968–5976. https://doi.org/10.1210/jc.2019-00721
92. Dambrova M, Makrecka-Kuka M, Kuka J, Vilskersts R, Nordberg D, Attwood MM, Smesny S, Sen ZD, Guo AC, Oler E, Tian S, Zheng J, Wishart DS, Liepinsh E, Schiöth HB. 2022. Acylcarnitines: nomenclature, biomarkers, therapeutic potential, drug targets, and clinical trials. Pharmacol Rev 74:506–551. https://doi.org/10.1124/pharmrev.121.000408
93. Rattray NJW, Trivedi DK, Xu Y, Chandola T, Johnson CH, Marshall AD, Mekli K, Rattray Z, Tampubolon G, Vanhoutte B, White IR, Wu FCW, Pendleton N, Nazroo J, Goodacre R. 2019. Metabolic dysregulation in vitamin E and carnitine shuttle energy mechanisms associate with human frailty. Nat Commun 10:5027. https://doi.org/10.1038/s41467-019-12716-2
94. Kolar MJ, Konduri S, Chang T, Wang H, McNerlin C, Ohlsson L, Härröd M, Siegel D, Saghatelian A. 2019. Linoleic acid esters of hydroxy linoleic acids are anti-inflammatory lipids found in plants and mammals. J Biol Chem 294:10698–10707. https://doi.org/10.1074/jbc.RA118.006956
95. Liberati-Čizmek A-M, Biluš M, Brkić AL, Barić IC, Bakula M, Hozić A, Cindrić M. 2019. Analysis of fatty acid esters of hydroxyl fatty acid in selected plant food. Plant Foods Hum Nutr 74:235–240. https://doi.org/10.1007/s11130-019-00728-8
96. Weibel DB, Shevy LE, Schroeder FC, Meinwald J. 2002. Synthesis of mayolene-16 and mayolene-18: larval defensive lipids from the European Cabbage butterfly. J Org Chem 67:5896–5900. https://doi.org/10.1021/jo011102q
97. Smedley SR, Schroeder FC, Weibel DB, Meinwald J, Lafleur KA, Renwick JA, Rutowski R, Eisner T. 2002. Mayolenes: labile defensive lipids from the glandular hairs of a caterpillar (*Pieris rapae*). Proc Natl Acad Sci U S A 99:6822–6827. https://doi.org/10.1073/pnas.102165699
98. Yore MM, Syed I, Moraes-Vieira PM, Zhang T, Herman MA, Homan EA, Patel RT, Lee J, Chen S, Peroni OD, Dhaneshwar AS, Hammarstedt A, Smith U, McGraw TE, Saghatelian A, Kahn BB. 2014. Discovery of a class of endogenous mammalian lipids with anti-diabetic and anti-inflammatory effects. Cell 159:318–332. https://doi.org/10.1016/j.cell.2014.09.035
99. Mendoza-Porras O, Nguyen TV, Shah RM, Thomas-Hall P, Bastin L, Deaker DJ, Motti CA, Byrne M, Beale DJ. 2023. Biochemical metabolomic profiling of the Crown-of-Thorns Starfish (*Acanthaster*): new insight into its biology for improved pest management. Sci Total Environ 861:160525. https://doi.org/10.1016/j.scitotenv.2022.160525
100. Vences-Guzmán MÁ, Geiger O, Sohlenkamp C. 2012. Ornithine lipids and their structural modifications: from A to E and beyond. FEMS Microbiol Lett 335:1–10. https://doi.org/10.1111/j.1574-6968.2012.02623.x
101. Kuda O, Brezinova M, Silhavy J, Landa V, Zidek V, Dodia C, Kreuchwig F, Vrbacky M, Balas L, Durand T, Hübner N, Fisher AB, Kopecky J, Pravenec M. 2018. Nrf2-mediated antioxidant defense and peroxiredoxin 6 are linked to biosynthesis of palmitic acid ester of 9-hydroxystearic acid. Diabetes 67:1190–1199. https://doi.org/10.2337/db17-1087
102. Wang M, Jarmusch AK, Vargas F, Aksenov AA, Gauglitz JM, Weldon K, Petras D, da Silva R, Quinn R, Melnik AV, et al. 2020. Mass spectrometry searches using MASST. Nat Biotechnol 38:23–26. https://doi.org/10.1038/s41587-019-0375-9
103. Pei J-Y, Yu W-F, Zhang J-J, Kuo T-H, Chung H-H, Hu J-J, Hsu C-C, Yu K-F. 2022. Mass spectrometry–based metabolomic signatures of coral bleaching under thermal stress. Anal Bioanal Chem 414:7635–7646. https://doi.org/10.1007/s00216-022-04294-y
104. Magtanong L, Ko P-J, To M, Cao JY, Forcina GC, Tarangelo A, Ward CC, Cho K, Patti GJ, Nomura DK, Olzmann JA, Dixon SJ. 2019. Exogenous monounsaturated fatty acids promote a ferroptosis-resistant cell state. Cell Chem Biol 26:420–432. https://doi.org/10.1016/j.chembiol.2018.11.016
105. Berkelmans R, van Oppen MJH. 2006. The role of zooxanthellae in the thermal tolerance of corals: a 'nugget of hope' for coral reefs in an era of climate change. Proc R Soc B 273:2305–2312. https://doi.org/10.1098/rspb.2006.3567
106. Rowan R. 2004. Thermal adaptation in reef coral symbionts. Nature 430:742. https://doi.org/10.1038/430742a
107. LaJeunesse TC, Wham DC, Pettay DT, Parkinson JE, Keshavmurthy S, Chen CA. 2014. Ecologically differentiated stress-tolerant endosymbionts in the dinoflagellate genus *Symbiodinium* (Dinophyceae) Clade D are different species. Phycologia 53:305–319. https://doi.org/10.2216/13-186.1
108. Silverstein RN, Cunning R, Baker AC. 2017. Tenacious D: *Symbiodinium* in clade D remain in reef corals at both high and low temperature extremes despite impairment. J Exp Biol 220:1192–1196. https://doi.org/10.1242/jeb.148239
109. Iglesias-Prieto R, Beltrán VH, LaJeunesse TC, Reyes-Bonilla H, Thomé PE. 2004. Different algal symbionts explain the vertical distribution of dominant reef corals in the eastern Pacific. Proc R Soc Lond B 271:1757–1763. https://doi.org/10.1098/rspb.2004.2757
110. Kemp DW, Hernandez-Pech X, Iglesias-Prieto R, Fitt WK, Schmidt GW. 2014. Community dynamics and physiology of *Symbiodinium* spp. before, during, and after a coral bleaching event. Limnol Oceanogr 59:788–797. https://doi.org/10.4319/lo.2014.59.3.0788
111. Rowan R, Knowlton N. 1995. Intraspecific diversity and ecological zonation in coral-algal symbiosis. Proc Natl Acad Sci USA 92:2850–2853. https://doi.org/10.1073/pnas.92.7.2850
112. Sikorskaya TV, Efimova KV, Imbs AB. 2021. Lipidomes of phylogenetically different symbiotic dinoflagellates of corals. Phytochemistry 181:112579. https://doi.org/10.1016/j.phytochem.2020.112579
113. Iba K. 2002. Acclimative response to temperature stress in higher plants: approaches of gene engineering for temperature tolerance. Annu Rev Plant Biol 53:225–245. https://doi.org/10.1146/annurev.arplant.53.100201.160729
114. Morgan-Kiss RM, Priscu JC, Pocock T, Gudynaite-Savitch L, Huner NPA. 2006. Adaptation and acclimation of photosynthetic microorganisms to permanently cold environments. Microbiol Mol Biol Rev 70:222–252. https://doi.org/10.1128/MMBR.70.1.222-252.2006
115. Oakley CA, Pontasch S, Fisher PL, Wilkinson SP, Keyzers RA, Krueger T, Dove S, Hoegh-Guldberg O, Leggat W, Davy SK. 2022. Thylakoid fatty acid composition and response to short-term cold and heat stress in high-latitude Symbiodiniaceae. Coral Reefs 41:343–353. https://doi.org/10.1007/s00338-022-02221-2
116. Johansen JE, Svec WA, Liaaen-Jensen S, Haxo FT. 1974. Carotenoids of the dinophyceae. Phytochemistry 13:2261–2271. https://doi.org/10.1016/0031-9422(74)85038-7
117. Takaichi S. 2011. Carotenoids in algae: distributions, biosyntheses and functions. Mar Drugs 9:1101–1118. https://doi.org/10.3390/md9061101
118. Wakahama T, Laza-Martínez A, Bin Haji Mohd Taha AI, Okuyama H, Yoshida K, Kogame K, Awai K, Kawachi M, Maoka T, Takaichi S. 2012. Structural confirmation of a unique carotenoid lactoside, P457, in *Symbiodinium* sp. strain nbrc 104787 isolated from a sea anemone and its distribution in dinoflagellates and various marine organisms. J Phycol 48:1392–1402. https://doi.org/10.1111/j.1529-8817.2012.01219.x
119. Ushijima B, Meyer JL, Thompson S, Pitts K, Marusich MF, Tittl J, Weatherup E, Reu J, Wetzell R, Aeby GS, Häse CC, Paul VJ. 2020. Disease diagnostics and potential coinfections by *Vibrio coralliilyticus* during an ongoing coral disease outbreak in Florida. Front Microbiol 11:569354. https://doi.org/10.3389/fmicb.2020.569354
120. Ushijima B, Gunasekera SP, Meyer JL, Tittl J, Pitts KA, Thompson S, Sneed JM, Ding Y, Chen M, Jay Houk L, Aeby GS, Häse CC, Paul VJ. 2023. Chemical and genomic characterization of a potential probiotic treatment for stony coral tissue loss disease. Commun Biol 6:248. https://doi.org/10.1038/s42003-023-04590-y
121. Grevengoed TJ, Trammell SAJ, McKinney MK, Petersen N, Cardone RL, Svenningsen JS, Ogasawara D, Nexøe-Larsen CC, Knop FK, Schwartz TW, Kibbey RG, Cravatt BF, Gillum MP. 2019. *N*-acyl taurines are endogenous lipid messengers that improve glucose homeostasis. Proc

Natl Acad Sci U S A 116:24770–24778. https://doi.org/10.1073/pnas.1916288116
122. Gauff RPM, Lejeusne C, Greff S, Loisel S, Bohner O, Davoult D. 2022. Impact of *in situ* simulated climate change on communities and non-indigenous species: two climates, two responses. J Chem Ecol 48:761–771. https://doi.org/10.1007/s10886-022-01380-4
123. Mohimani H, Gurevich A, Shlemov A, Mikheenko A, Korobeynikov A, Cao L, Shcherbin E, Nothias L-F, Dorrestein PC, Pevzner PA. 2018. Dereplication of microbial metabolites through database search of mass spectra. Nat Commun 9:4035. https://doi.org/10.1038/s41467-018-06082-8
124. Matthews JL, Cunning R, Ritson-Williams R, Oakley CA, Lutz A, Roessner U, Grossman AR, Weis VM, Gates RD, Davy SK. 2020. Metabolite pools of the reef building coral *Montipora capitata* are unaffected by Symbiodiniaceae community composition. Coral Reefs 39:1727–1737. https://doi.org/10.1007/s00338-020-01999-3
125. Gantt A. 2021. Stony coral tissue loss disease found at Dry Tortugas National Park. Available from: https://www.nps.gov/drto/learn/news/stony-coral-tissue-loss-disease-found-at-dry-tortugas-national-park.htm#:~:text=KEY%20WEST%2C%20Fla.,conducting%20a%20routine%20disease%20survey
126. Pluskal T, Castillo S, Villar-Briones A, Orešič M. 2010. MZmine 2: modular framework for processing, visualizing, and analyzing mass spectrometry-based molecular profile data. BMC Bioinformatics 11:395. https://doi.org/10.1186/1471-2105-11-395
127. Wang M, Carver JJ, Phelan VV, Sanchez LM, Garg N, Peng Y, Nguyen DD, Watrous J, Kapono CA, Luzzatto-Knaan T, et al. 2016. Sharing and community curation of mass spectrometry data with Global Natural Products Social Molecular Networking. Nat Biotechnol 34:828–837. https://doi.org/10.1038/nbt.3597
128. Nothias L-F, Petras D, Schmid R, Dührkop K, Rainer J, Sarvepalli A, Protsyuk I, Ernst M, Tsugawa H, Fleischauer M, et al. 2020. Feature-based molecular networking in the GNPS analysis environment. Nat Methods 17:905–908. https://doi.org/10.1038/s41592-020-0933-6
129. Dührkop K, Fleischauer M, Ludwig M, Aksenov AA, Melnik AV, Meusel M, Dorrestein PC, Rousu J, Böcker S. 2019. SIRIUS 4: a rapid tool for turning tandem mass spectra into metabolite structure information. Nat Methods 16:299–302. https://doi.org/10.1038/s41592-019-0344-8
130. Shannon P, Markiel A, Ozier O, Baliga NS, Wang JT, Ramage D, Amin N, Schwikowski B, Ideker T. 2003. Cytoscape: a software environment for integrated models of biomolecular interaction networks. Genome Res 13:2498–2504. https://doi.org/10.1101/gr.1239303
131. van der Hooft JJJ, Wandy J, Young F, Padmanabhan S, Gerasimidis K, Burgess KEV, Barrett MP, Rogers S. 2017. Unsupervised discovery and comparison of structural families across multiple samples in untargeted metabolomics. Anal Chem 89:7569–7577. https://doi.org/10.1021/acs.analchem.7b01391
132. McAvoy AC, Jaiyesimi O, Threatt PH, Seladi T, Goldberg JB, da Silva RR, Garg N. 2020. Differences in cystic fibrosis-associated *Burkholderia* spp. bacteria metabolomes after exposure to the antibiotic Trimethoprim. ACS Infect Dis 6:1154–1168. https://doi.org/10.1021/acsinfecdis.9b00513
133. Jarmusch AK, Aron AT, Petras D, Phelan VV, Bittremieux W, Acharya DD, Ahmed MMA, Bauermeister A, Bertin MJ, Boudreau PD, et al. 2022. A universal language for finding mass spectrometry data patterns. bioRxiv. https://doi.org/10.1101/2022.08.06.503000
134. Cao L, Guler M, Tagirdzhanov A, Lee Y-Y, Gurevich A, Mohimani H. 2021. MolDiscovery: learning mass spectrometry fragmentation of small molecules. Nat Commun 12:3718. https://doi.org/10.1038/s41467-021-23986-0
135. Sumner LW, Amberg A, Barrett D, Beale MH, Beger R, Daykin CA, Fan TWM, Fiehn O, Goodacre R, Griffin JL, Hankemeier T, Hardy N, Harnly J, Higashi R, Kopka J, Lane AN, Lindon JC, Marriott P, Nicholls AW, Reily MD, Thaden JJ, Viant MR. 2007. Proposed minimum reporting standards for chemical analysis. Metabolomics (Los Angel) 3:211–221. https://doi.org/10.1007/s11306-007-0082-2
136. Jolliffe IT. 1986. Principal component analysis. Springer.
137. Ward JH. 1963. Hierarchical grouping to optimize an objective function. J Am Stat Assoc 58:236–244. https://doi.org/10.1080/01621459.1963.10500845
138. Pang Z, Chong J, Zhou G, de Lima Morais DA, Chang L, Barrette M, Gauthier C, Jacques P-É, Li S, Xia J. 2021. MetaboAnalyst 5.0: narrowing the gap between raw spectra and functional insights. Nucleic Acids Res 49:W388–W396. https://doi.org/10.1093/nar/gkab382
139. Khan A, Mathelier A. 2017. Intervene: a tool for intersection and visualization of multiple gene or genomic region sets. BMC Bioinformatics 18:287. https://doi.org/10.1186/s12859-017-1708-7
140. Bray JR, Curtis JT. 1957. An ordination of the upland forest communities of southern Wisconsin. Ecol Monogr 27:325–349. https://doi.org/10.2307/1942268
141. Kruskal JB, Wish M. 1978. Multidimensional scaling, p 7–11. Sage Publications, Newbury Park.
142. Clarke KR, Gorley RN. 2015. PRIMER v7:PRIMER-EPlymouth
143. Anderson MJ. 2006. Distance-based tests for homogeneity of multivariate dispersions. Biometrics 62:245–253. https://doi.org/10.1111/j.1541-0420.2005.00440.x
144. Shannon CE. 1948. A mathematical theory of communication. Bell Syst Tech J 27:379–423. https://doi.org/10.1002/j.1538-7305.1948.tb01338.x
145. Gower JC. 1966. Some distance properties of latent root and vector methods used in multivariate analysis. Biometrika 53:325. https://doi.org/10.2307/2333639
146. Dührkop K, Shen H, Meusel M, Rousu J, Böcker S. 2015. Searching molecular structure databases with tandem mass spectra using CSI:FingerID. Proc Natl Acad Sci U S A 112:12580–12585. https://doi.org/10.1073/pnas.1509788112
147. Dührkop K, Nothias L-F, Fleischauer M, Reher R, Ludwig M, Hoffmann MA, Petras D, Gerwick WH, Rousu J, Dorrestein PC, Böcker S. 2021. Systematic classification of unknown metabolites using high-resolution fragmentation mass spectra. Nat Biotechnol 39:462–471. https://doi.org/10.1038/s41587-020-0740-8
148. Wandy J, Zhu Y, van der Hooft JJJ, Daly R, Barrett MP, Rogers S. 2018. Ms2lda.org: web-based topic modelling for substructure discovery in mass spectrometry. Bioinformatics 34:317–318. https://doi.org/10.1093/bioinformatics/btx582
149. Yan X, Markey SP, Marupaka R, Dong Q, Cooper BT, Mirokhin YA, Wallace WE, Stein SE. 2020. Mass spectral library of acylcarnitines derived from human urine. Anal Chem 92:6521–6528. https://doi.org/10.1021/acs.analchem.0c00129